

Development of Novel Photocatalyst and Cocatalyst Materials for Water Splitting under Visible Light

Kazuhiko Maeda*¹ and Kazunari Domen²

¹Department of Chemistry, Graduate School of Science and Engineering, Tokyo Institute of Technology, 2-12-1-NE-2 Ookayama, Meguro-ku, Tokyo 152-8550

²Department of Chemical System Engineering, The University of Tokyo, 7-3-1 Hongo, Bunkyo-ku, Tokyo 113-8656
E-mail: maedak@chem.titech.ac.jp

Received: December 22, 2015; Accepted: January 12, 2016; Web Released: January 18, 2016



Kazuhiko Maeda

Kazuhiko Maeda received his B.Sc. from Tokyo University of Science (2003), M.Sc. from Tokyo Institute of Technology (2005), and Ph.D. from The University of Tokyo (2007). During 2008–2009, he was a Postdoctoral Fellow at Pennsylvania State University. He then joined The University of Tokyo as an Assistant Professor in 2009. Moving to Tokyo Institute of Technology in 2012, he was promoted to Associate Professor. He was also appointed as a PRESTO/JST researcher during 2010–2014. His major research interest is heterogeneous photocatalysis for light to chemical energy conversion, with a focus on water splitting and CO₂ fixation.



Kazunari Domen

Kazunari Domen received his B.Sc. (1976), M.Sc. (1979), and Ph.D. (1982) in chemistry from The University of Tokyo. He joined the Tokyo Institute of Technology in 1982 as an Assistant Professor and was subsequently promoted to Associate Professor in 1990 and Full Professor in 1996. He moved to The University of Tokyo in 2004 and is currently a Full Professor. His current research interests include heterogeneous photocatalysis and photoelectrochemistry for water splitting.

Abstract

Overall water splitting using a semiconductor photocatalyst with sunlight has long been viewed as a potential means of large-scale H₂ production from renewable resources. In general, the reaction can be accomplished when a photocatalyst is modified with a suitable cocatalyst that efficiently promotes water reduction. It is therefore essential to develop both photocatalysts and cocatalysts in harmony. Certain metal (oxy)-nitrides are potential candidates as water-splitting photocatalysts because of their suitable band edge positions for water reduction/oxidation, small band gaps (<3 eV), and stability under irradiation. However, efficient water splitting using visible-light-responsive oxynitrides has still remained a challenge. This account describes our recent developments over the last 10 years of new oxynitrides as well as cocatalysts for overall water splitting under visible light.

1. Introduction

1.1 Research Background. The production of H₂ from water and sunlight using heterogeneous semiconductor photocatalysts is a promising means of addressing the depletion of fossil fuels and the serious environmental problems accompanying their combustion.^{1–10} Water splitting into H₂ and O₂ (eq 1) is a typical “uphill reaction”, involving a large positive change in the Gibbs energy ($\Delta G^\circ = 238 \text{ kJ mol}^{-1}$).



This research was initially triggered by the demonstration of photoelectrochemical (PEC) water splitting using a single-crystal TiO₂ (rutile) photoanode and a Pt cathode with a chemical bias, which is well known as the Honda–Fujishima effect.¹¹ So far, numerous PEC cells have been developed, many of which were designed specifically for the efficient utilization of solar energy.^{4,8,10,12,13} Due to the lack of suitable photoelec-

trode materials with appropriate band-gap structures and stability, however, the PEC systems developed to date have been rather complicated, such as integrated multilayer and tandem systems.

Overall water splitting for H₂ production on a semiconductor particle, similar in many ways to the photosynthetic reaction, has been studied since 1980.^{14–16} According to our assessment, it was suggested that for practical future applications, an area of 250000 km², corresponding to 1% of the earth's desert area, would be required to provide one-third of the projected energy needs of human society in 2050 from solar energy, assuming a conversion efficiency of 10% and an integrated solar energy of AM1.5G (1 sun = 100 mW cm⁻²) irradiation for a day including a sunlight-angle correction.¹⁷ Although a method for separating the simultaneously produced H₂ and O₂ remains to be developed, particulate photocatalyst systems have a wider range of potential applications from the viewpoint of such large-scale hydrogen production.

1.2 Basic Principles of Water Splitting on a Semiconductor Particle. Figure 1 illustrates the basic principle of

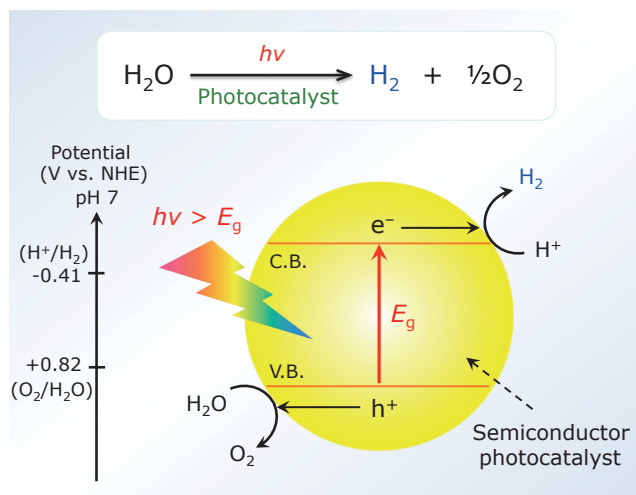


Figure 1. Schematic energy diagram of overall water splitting on a semiconductor photocatalyst. V.B. and C.B. mean valence band and conduction band, respectively. E_g indicates the band-gap energy of a semiconductor photocatalyst.

overall water splitting on a semiconductor particle. When a semiconductor photocatalyst absorbs light energy equivalent to or greater than the band gap of the photocatalyst, electrons in the valence band are excited into the conduction band, leaving holes in the valence band. The photogenerated electrons and holes cause reduction and oxidation reactions, respectively. To achieve overall water splitting into H₂ and O₂, the conduction band minimum (CBM) must be more negative than the reduction potential of H⁺ to H₂ (0 V vs. NHE at pH 0), while the valence band maximum (VBM) must be more positive than the oxidation potential of H₂O to O₂ (1.23 V vs. NHE). Therefore, the minimum photon energy thermodynamically required to drive photocatalytic water splitting is 1.23 eV, which corresponds to a wavelength of ca. 1000 nm. Accordingly, it is essentially possible to utilize the entire spectral range of visible light (400 < λ < 800 nm). However, there is an activation barrier in the charge-transfer process between the solid photocatalyst and water molecules, requiring a photon energy greater than the band gap of the photocatalyst to drive the overall water-splitting reaction at a reasonable rate. As will be described later, cocatalysts play a vital role in the charge-transfer reaction at the solid-liquid interface. In addition, backward reactions of thermodynamically more oxidizable and reducible products (e.g., water formation from H₂ and O₂), must be strictly inhibited, and the photocatalysts themselves need to work stably in the reaction. Furthermore, although there are a large number of materials that possess suitable band-gap potentials, there are very few that function as photocatalysts for overall water splitting, due to other factors that will be discussed below.

1.3 Factors Affecting Photocatalytic Activity. As shown in Figure 2, overall water splitting on a semiconductor photocatalyst, typically with the size of several hundreds of nanometers to several micrometers, occurs in three steps: (1) the photocatalyst absorbs light energy greater than the band-gap energy of the material, generating photoexcited electron-hole pairs in the bulk material, (2) the photogenerated carriers separate and move to the surface without recombination, and (3) adsorbed species undergo reduction and oxidation by reaction with the photogenerated electrons and holes to produce H₂ and O₂, respectively. The first two steps depend strongly on the structural and electronic properties of the semiconductor photocatalyst. High crystallinity in general has a positive impact on

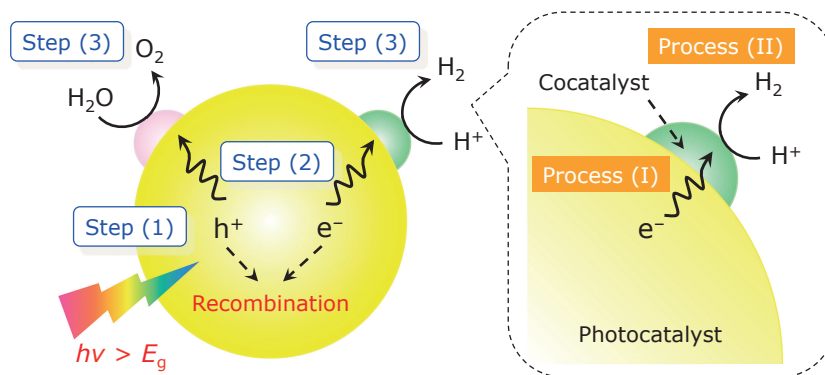


Figure 2. Processes involved in photocatalytic overall water splitting on a semiconductor particle. A schematic illustration of electron transfer from a photocatalyst to the loaded cocatalyst (Process I) and H₂ evolution (Process II) in the reaction is also shown.

activity, because the density of defects, which serve as recombination centers between photogenerated electrons and holes, decreases with increasing crystallinity. One can also enhance photocatalytic activity by reducing the particle size of a photocatalyst, because the diffusion length for photogenerated electron–hole pairs can be shortened. On the other hand, the third step is promoted by a cocatalyst loaded on the photocatalyst surface. The cocatalyst is typically a noble metal (e.g., Pt, Rh) or transition metal oxide (e.g., NiO_x, RuO₂) and is loaded onto the photocatalyst surface as a dispersion of nanoparticles (typically <50 nm in size) to produce active sites and reduce the activation energy for gas evolution.^{2,6,17} In most cases, cocatalysts are loaded for the promotion of H₂ evolution, presumably because most photocatalysts are unable to activate hydrogen on the surface. As illustrated in Figure 2, the loaded cocatalysts extract photogenerated electrons from the photocatalyst (process I) and host active sites for gas evolution (process II). Therefore, the overall efficiency of a given photocatalytic system is dependent on the loaded cocatalyst. In particular, the structural characteristics and intrinsic catalytic properties of a cocatalyst for H₂ (or O₂) evolution are important. For example, Pt is well known as an excellent reduction catalyst of protons to form H₂ molecules. However, a photocatalyst modified with a Pt cocatalyst does not always show the highest activity among analogues loaded with other metals (e.g., Ru and Rh). This suggests that the contribution of process (I) to the overall efficiency can be more important than that of process (II). For example, Ru-loaded TaON was reported to give a much higher activity for H₂ evolution from aqueous methanol solution than a Pt-loaded one.¹⁸ Because no report has yielded a systematic understanding of which process, I or II, is more important in a specific case, one must consider both processes when designing an efficient photocatalytic system. It is thus important to design both the bulk and surface properties of the material carefully so as to obtain a high activity for photocatalytic overall water splitting.

Since overall water splitting is generally difficult to achieve due to the uphill nature of the reaction, photocatalytic activities of a given compound for water reduction or oxidation are usually examined individually in the presence of methanol or silver nitrate as a sacrificial reagent. Reactions using sacrificial reagents are not “overall” water-splitting reactions, but are often carried out as test reactions for overall water splitting. The basic principle of photocatalytic reactions using sacrificial reagents is displayed schematically in Figure 3. When the photocatalytic reaction is conducted in the presence of an

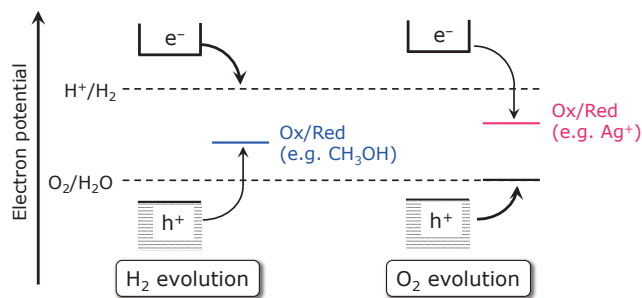


Figure 3. Basic principle of photocatalytic reactions in the presence of sacrificial reagents.

electron donor such as methanol, photogenerated holes in the valence band irreversibly oxidize methanol instead of H₂O, thus facilitating water reduction by conduction band electrons if the bottom of the conduction band of the photocatalyst is located above the water reduction potential. On the other hand, in the presence of an electron acceptor such as a silver cation, photogenerated electrons in the conduction band irreversibly reduce electron acceptors instead of H⁺, thereby promoting water oxidation by valence band holes if the top of the valence band of the photocatalyst is more positive than the water oxidation potential. However, it should be noted that the ability of a photocatalyst to both reduce and oxidize water separately does not guarantee its capability to achieve overall water splitting without sacrificial reagents.

1.4 (Oxy)nitrides as Visible-Light-Driven Photocatalysts.

Development of a photocatalyst that splits water efficiently under visible light ($\lambda > 400$ nm) is necessary from the viewpoint of solar energy utilization. The major obstacle to the development of powder photocatalysts has been the lack of a photocatalyst that satisfies the following three requirements: (1) a band gap smaller than 3 eV, (2) band-edge potentials suitable for overall water splitting, and (3) stability in the photocatalytic reaction. Many metal oxides have already been reported to work as highly efficient photocatalysts for overall water splitting with apparent quantum yields (AQYs) of several tens of percent.^{19–23} However, most of them essentially work under UV irradiation due to their large band gaps (>3 eV).

In the development of such a photocatalyst, it is especially important to control the band structure. In UV-active metal oxide photocatalysts, the CBM, which consists mainly of empty transition-metal d orbitals, is located at a potential slightly more negative than 0 V (vs. NHE) at pH 0, and the VBM, consisting of O2p orbitals, is more positive than 3 V.²⁴ This situation creates a band gap of the metal oxide material that is too large to harvest visible light, although there are several examples of metal oxides showing visible-light water reduction/oxidation activities.^{3,6} Nevertheless, it suggests that metal oxide photocatalysts have enough potential to oxidize water, judging from the difference between the oxidation potential of H₂O into O₂ (1.23 V vs. NHE) and the VBM (ca. 3 V vs. NHE).

Since the N2p orbital has a higher potential energy than the O2p orbital, using a metal nitride or oxynitride as a photocatalyst is of interest. It is noted that this type of material differs from materials doped with nitrogen,²⁵ because nitrogen is contained as the principal anionic component and forms not an impurity level but a constituent valence band. Figure 4 shows the schematic band structures of a metal oxide (NaTaO₃) and oxynitride (BaTaO₂N), both of which have the same perovskite structure. The VBM for the metal oxide consists of O2p orbitals. When N atoms are partially or fully substituted for O atoms in a metal oxide, the VBM of the material is expected to shift higher compared to the corresponding metal oxide, without affecting the CBM. As expected, density functional theory (DFT) calculations for BaTaO₂N have indicated that the VBM consists of hybridized N2p and O2p orbitals, whereas the CBM is mainly composed of empty Ta5d orbitals.² The potential of the VBM for the oxynitride lies at higher potential energy than that for the corresponding oxide material due to the

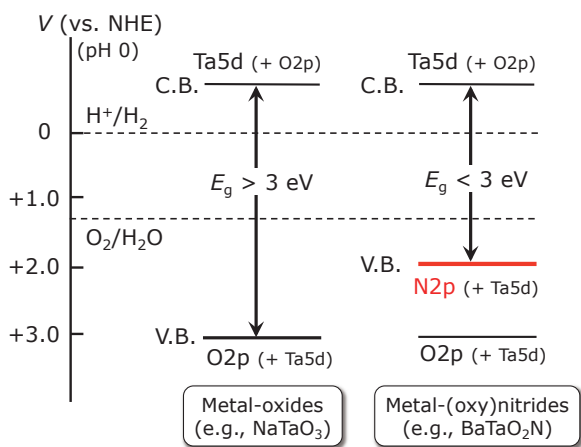


Figure 4. Schematic band structures of a metal oxide (NaTaO_3) and metal (oxy)nitride (BaTaO_2N).

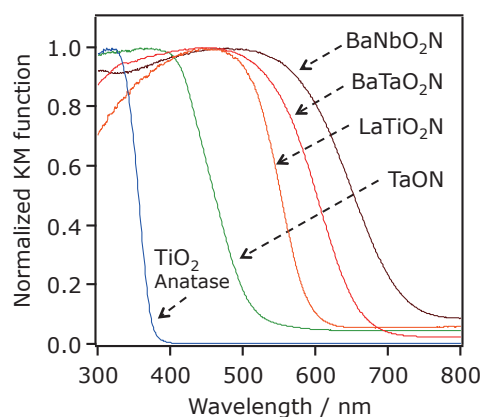


Figure 5. UV-visible diffuse reflectance spectra for (oxy)nitrides containing Ti^{4+} , Nb^{5+} , and Ta^{5+} .

contribution of $\text{N}2\text{p}$ orbitals, making the band gap energy sufficiently small to respond to visible light (<3 eV).

1.5 Early Work. Some particulate (oxy)nitrides containing early transition-metal cations are stable and non-toxic materials, and can be readily obtained by nitriding a corresponding metal oxide powder. They have recently attracted attention as chemically stable (except in strong acids), non-toxic inorganic pigment alternatives to chalcogenides-based pigments.²⁶ Our group has been developing (oxy)nitrides as photocatalysts for water splitting under visible light.² Since the initial reports published in 2002,^{27–30} a variety of (oxy)nitrides with d^0 electronic configurations have been reported as candidates for photocatalytic water splitting under visible light.³¹ Figure 5 shows UV-visible diffuse reflectance spectra of some d^0 - (oxy)nitrides. It is clear that these (oxy)nitrides possess absorption bands at 500–750 nm, corresponding to band gaps of 1.7–2.5 eV that are estimated from the onset wavelengths of the absorption spectra. Under visible-light irradiation, they are capable of producing H_2 and O_2 individually in the presence of suitable electron donors and acceptors, respectively, without noticeable degradation. However, overall water splitting using these d^0 - (oxy)nitrides was not achieved until 2005, as mentioned in the latter section. Therefore, overall water splitting on a semiconductor particle by visible light had been once described as one of the “Holy Grails” of chemistry.³²

1.6 Scope of This Account. Owing to recent rising interest in photocatalytic water splitting, many reviews and accounts have been published.^{1–10} In order to avoid redundant discussion in the present account, the authors will focus on photocatalyst and cocatalyst materials developed by the same authors’ group in the last 10 years toward efficient water splitting under visible light. In the next section, solid solutions of GaN and ZnO are introduced as the first successful example of a visible-light-responsive photocatalyst that is active for overall water splitting. Next, the discussion moves to a description of how the photocatalytic activity of GaN:ZnO solid solutions can be improved, with a focus on cocatalysts to promote the water reduction process. In the last section, activation of d^0 -type oxynitrides that aims to utilize more visible photons is discussed.

2. GaN:ZnO Solid Solutions

2.1 Development of (Oxy)nitrides with d^{10} Electronic Configuration. In terms of electronic band structure, d^{10} -semiconductors containing typical metal cations have an advantage as photocatalysts, compared to materials with d^0 electronic configurations.³³ The VBM of transition metal oxides with a d^0 electronic configuration consists of $\text{O}2\text{p}$ orbitals, while the CBM is composed of empty d orbitals of the transition metals. In typical metal oxides with a d^0 electronic configuration, however, the CBM consists of hybridized s,p orbitals of the metals, although the VBM is essentially formed by $\text{O}2\text{p}$ orbitals. The hybridized s,p orbitals have large dispersion, increasing the mobility of photogenerated electrons in the conduction band and promoting photocatalytic activity.³³

Inspired by this hypothesis, (oxy)nitrides with a d^{10} electronic configuration are of interest as potentially efficient photocatalysts for overall water splitting, and $\beta\text{-Ge}_3\text{N}_4$ modified with RuO_2 nanoparticle cocatalysts was found to function as a photocatalyst for overall water splitting.³⁴ This was the first example of a non-oxide photocatalyst capable of splitting pure water into H_2 and O_2 . Follow-up studies have investigated effects of post-treatment to enhance the activity of $\beta\text{-Ge}_3\text{N}_4$ and its photocatalytic properties.^{35,36} The relationship between the structural characteristics and the photocatalytic performance of $\beta\text{-Ge}_3\text{N}_4$ has also been investigated.³⁷ Unfortunately, the band gap of $\beta\text{-Ge}_3\text{N}_4$ is approximately 3.8 eV, which is sensitive only to ultraviolet light.³⁶

2.2 Initial Concept for Developing GaN:ZnO Solid Solutions. To devise a new d^{10} - (oxy)nitride with a visible-light response, we focused on gallium nitride (GaN), which is well known as a light-functional material for applications in light-emitting diodes and laser diodes. Although the VBM and CBM straddle the water reduction/oxidation potentials, its large band gap (ca. 3.4 eV) restricts its use of visible photons.^{38–40} Nevertheless, we believed that this situation could be overcome by the following strategy. For II–VI semiconductors containing $\text{Zn}2\text{p}$ ions as a principal component (e.g., ZnAl_2O_4), it has been reported that a repulsive interaction between $\text{O}2\text{p}$ and $\text{Zn}3\text{d}$ orbitals shifts the VBM upward without affecting the CBM.⁴¹ Similarly, we thought that $p\text{-}d$ repulsion may occur when a Zn(II) compound is incorporated into the GaN lattice, causing the VBM formed by the $\text{N}2\text{p}$ atomic orbitals to rise to a higher potential energy (i.e., $\text{N}2\text{p}\text{-Zn}3\text{d}$ repulsion),

narrowing the band gap for GaN. The expected band structure of GaN:ZnO solid solution is illustrated in Figure 6A. Because both GaN and ZnO have wurtzite structures with similar lattice parameters,^{42,43} a solid solution can be formed

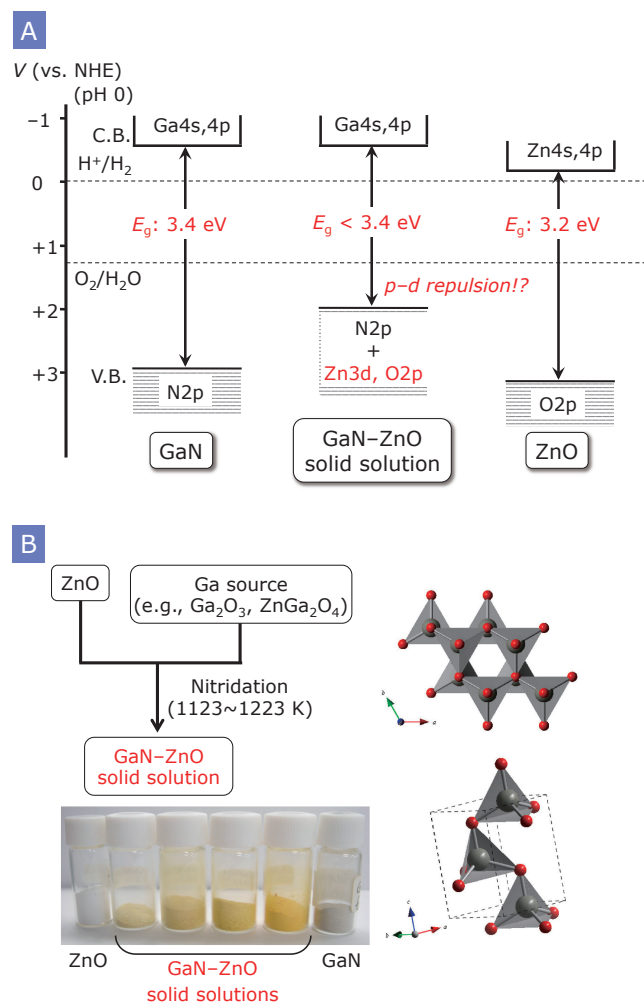


Figure 6. (A) Schematic illustration of the expected band structure of GaN-ZnO solid solution and (B) preparation scheme of the solid solution.

between the two. In this context, we chose ZnO as the paired compound for GaN to form a solid solution with visible-light response.

2.3 Synthesis of GaN:ZnO Solid Solutions. Preparation of the solid solution was first attempted by nitriding a mixture of a proper Ga source (e.g., Ga₂O₃) and ZnO under a flow of ammonia at ca. 1223 K.^{44,45} As shown in Figure 6B, the as-obtained products were yellow powders, depending on the preparation conditions. The yellow color clearly indicates visible-light absorption by this material, consistent with the initial hypothesis. Elemental analysis by inductive coupled plasma optical emission spectroscopy (ICP-OES) revealed that the ratios of Ga to N and Zn to O were close to 1, and that the nitrogen and oxygen concentrations increased with increasing gallium and zinc concentrations. X-ray diffraction (XRD) and neutron powder diffraction analyses indicated that the prepared samples are wurtzite solid solutions of GaN and ZnO with no interstitial sites and no large disorder in the material.⁴⁶

Based on these structural characterizations, it was concluded that the obtained material was indeed a solid solution of GaN and ZnO. The ideal composition of the solid solutions can be expressed as (Ga_{1-x}Zn_x)(N_{1-x}O_x), although the real compositions are somewhat deviated from the ideal one.⁴⁴ In this article, they are termed GaN:ZnO for simplicity. The specific compositions can be found in the cited literature.

2.4 The Origin of Visible-Light Response of GaN:ZnO Solid Solutions. Taking into account the large band-gap energies of GaN and ZnO (>3 eV), it was believed that the band gap of the solid solution should exceed 3 eV, despite the formation of the solid solution, as mentioned above. Interestingly, however, the GaN:ZnO solid solution had absorption edges in the visible region. Figure 7A shows UV-visible diffuse reflectance spectra of several GaN:ZnO samples with different compositions. The absorption edge shifted to longer wavelengths with increasing Zn and O concentrations in GaN:ZnO, clearly indicating that the visible-light response originated from the ZnO component in the material. The band-gap energies of the solid solutions were estimated to be 2.4–2.8 eV based on the diffuse reflectance spectra.

Initially, we thought that the origin of the visible-light absorption was the band-gap narrowing of GaN due to p-d

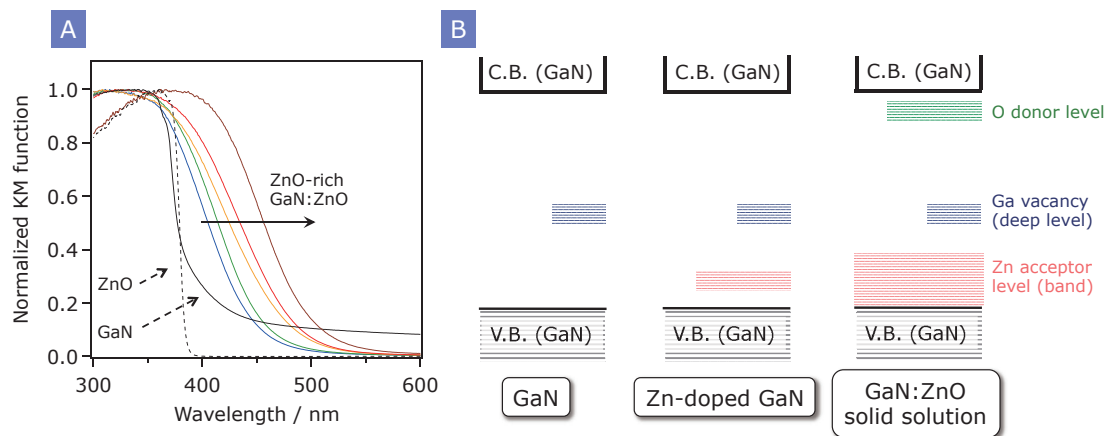


Figure 7. (A) Diffuse reflectance spectra of GaN:ZnO solid solutions with different compositions and (B) expected energy level diagrams for impurity levels in undoped GaN, Zn-doped GaN, and GaN-rich GaN:ZnO solid solutions.

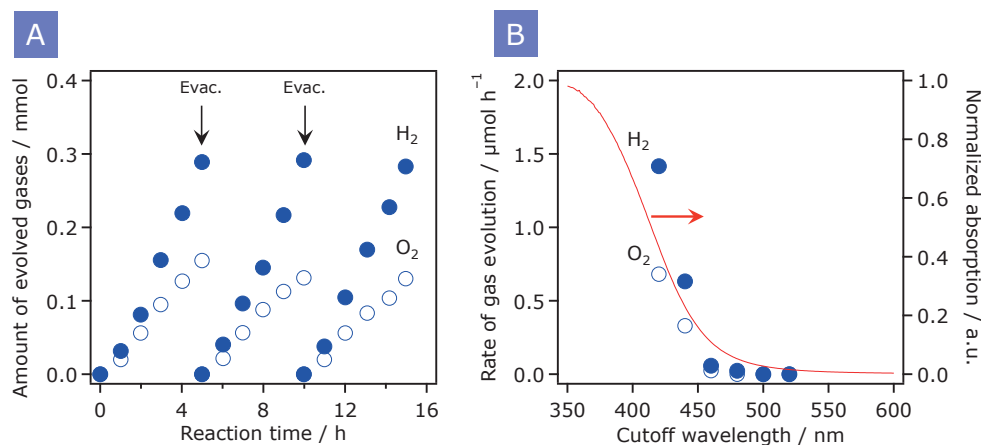


Figure 8. (A) Time course of overall water splitting using RuO₂-loaded GaN:ZnO under visible light ($\lambda > 400$ nm). (B) Dependence of water-splitting activity of RuO₂/GaN:ZnO on the wavelength of incident light. Reproduced from refs 44 and 49 with permission. Copyright 2005 and 2010 American Chemical Society.

repulsion between Zn3d and N2p electrons in the upper part of the valence band.^{44–46} However, our follow-up studies on the electronic structure of GaN-rich GaN:ZnO using photoluminescence spectroscopy and DFT calculations suggested that this material absorbs visible light via electron transitions from the Zn acceptor level to the conduction band while maintaining the band-gap structure of the host GaN, as illustrated in Figure 7B.^{47,48} Because the concentration of Zn in GaN:ZnO is relatively high, the acceptor level, which is filled with electrons derived from O donor levels (or thermal excitation), is likely to behave as an impurity band with a high density of states. Electrons can thus be transferred from the Zn acceptor level to the conduction band by visible-light absorption.

2.5 Relationship between Structure and Activity. The as-prepared GaN:ZnO exhibited little photocatalytic activity for water decomposition even under UV irradiation. However, modification by nanoparticulate cocatalysts that work as H₂ evolution sites (e.g., RuO₂ and NiO) resulted in clearly observable H₂ and O₂ evolution. Figure 8A shows a typical time course of overall water splitting on GaN:ZnO loaded with 5 wt% RuO₂ under visible irradiation ($\lambda > 400$ nm). No reaction took place in the dark, while both H₂ and O₂ evolved steadily and stoichiometrically upon visible-light irradiation. It has been reported that O₂ evolution occurs on a ZnO electrode as a result of degradation when employed as a photoanode for water oxidation in a PEC cell.⁵⁰ In this case, it was confirmed through ¹⁸O-isotopic H₂O cleavage experiments that the observed O₂ evolution on the solid solution was due to water oxidation, and the XRD pattern of the sample remained unchanged after the reaction. Figure 8B shows the dependence of the rate of H₂ and O₂ evolution on the wavelength of incident light. The H₂ and O₂ evolution rates both decreased as the cutoff wavelength increased. The longest wavelength available for the water-splitting reaction was 460 nm, corresponding to the absorption edge of the catalyst. These results indicate that GaN:ZnO functions as a stable photocatalyst for overall water splitting under visible light.

In general, the photocatalytic activity of conventional metal oxide photocatalysts for overall water splitting is known to depend strongly on the crystallinity and particle size of the

material, as determined by the preparation conditions.⁶ Therefore, investigating the physical factors that govern photocatalytic activity is an important and indispensable issue in the development of highly active photocatalysts. We thus investigated how the physicochemical properties of GaN:ZnO and preparation conditions affect photocatalytic activity for overall water splitting.^{45,49,51,52}

As illustrated in Figure 6B, the material could be readily prepared by nitriding a mixture of ZnO and an appropriate Ga-source at temperatures above 1123 K under a flow of NH₃. It was found that the addition of ZnO to the starting material promotes crystallization of GaN:ZnO and controls the zinc concentration, thereby improving activity. Accompanied with the crystallization, the concentration of ZnO tended to decrease. The release of ZnO from GaN:ZnO during the preparation process occurred as a result of reduction of Zn²⁺ cations and subsequent volatilization of Zn, generating defects and/or vacancies in the final product, which reduced photocatalytic activity.^{45,49,51} This situation was more pronounced when the synthesis was conducted under harsh conditions such as high temperatures and extended durations. By adjusting the nitridation conditions and the ratio of ZnO to the Ga source, it is possible to obtain a material with optimal crystallinity and atomic composition for overall water splitting under visible light. Structural analyses uncovered that the photocatalytic activity of GaN:ZnO for overall water splitting depends on the crystallinity and composition of the material, regardless of the kind of starting materials.^{45,49,51,52} More information on the preparation and performance of GaN:ZnO is available in our review paper.⁴⁹

2.6 Photocatalytic Activities in the Presence of Sacrificial Reagents. While most of the (oxy)nitride materials examined to date exhibit visible-light photocatalytic activity for such half reactions in the presence of a sacrificial reagent,² there are only a few materials that are capable of splitting pure water under visible light with sufficient reproducibility.⁶ Since half reactions are conducted as test reactions for overall water splitting, comparison of the activities for the half reactions with those for overall water splitting is of interest and is expected to provide useful information for the development of efficient photo-

Table 1. Photocatalytic activities of GaN:ZnO loaded with a transition-metal oxide and Cr oxide for overall water splitting under UV irradiation ($\lambda > 300 \text{ nm}$)^{a)}

Entry	Cocatalyst		Activity / $\mu\text{mol h}^{-1}$		Coloading amount of Cr /wt %	Activity of coloaded catalysts/ $\mu\text{mol h}^{-1}$	
	Element ^{b)}	Loading amount/wt %	H ₂	O ₂		H ₂	O ₂
1	None		0	0			
2	Cr	1.0	0	0			
3	Fe	1.0	0	0	1.0	73	36
4	Co	1.0	2.0	0	1.0	48	24
5	Ni	1.25	126	57	0.125	685	336
6	Cu	1.0	2.0	0	1.0	585	292
7	Ru	1.0	71	27	0.1	181	84
8	Rh	1.0	50	1.6	1.5	3835	1988
9	Pd	1.0	1.0	0	0.1	205	96
10	Ag	1.0	0	0	1.0	11	2.3
11	Ir	1.5	9.3	3.1	0.1	41	17
12	Pt	1.0	0.9	0.4	1.0	775	357

a) Catalyst (0.3 g); distilled water (370–400 mL); light source, high-pressure mercury lamp (450 W); inner irradiation-type reaction vessel made of Pyrex. b) Transition-metal species are expressed as metallic form for simplicity. Reproduced from ref 58 with permission.

catalysts. However, no comparative study had been made for visible-light-responsive photocatalysts.

Therefore, we conducted a systematic analysis of the dependence of the activities of GaN:ZnO for H₂ and O₂ evolution half reactions in the presence of sacrificial reagents on structural properties, and the results are compared to the data for overall water splitting.⁵³ GaN:ZnO evolved H₂ steadily from an aqueous methanol solution when loaded with a proper H₂ evolution cocatalyst, and evolved O₂ from an aqueous silver nitrate solution without the aid of a cocatalyst. Structural analyses indicated that the H₂ evolution activity depends strongly on the crystallinity and composition of GaN:ZnO, while the rate of O₂ evolution is proportionally related to the specific surface area. The activity for H₂ evolution from a methanol solution was of the same order as for overall water splitting, but was an order of magnitude lower than that for O₂ evolution from a silver nitrate solution. The results of photocatalytic reactions and PEC measurements suggested that the rate-determining step for overall water splitting using GaN:ZnO is the H₂ evolution process.

3. New Cocatalysts for Photocatalytic Overall Water Splitting

3.1 Cr(III)-Containing Transition Metal Oxides. NiO_x and RuO₂ are the most used cocatalysts for many photocatalysts, and no cocatalyst more effective than NiO_x or RuO₂ was found until 2006. It was reported by Domen et al. in 2000 that the photocatalytic activity of Ni-loaded K₂La₂Ti₃O₁₀ for overall water splitting could be improved by coloaded with Cr, while modification with Cr alone did not result in appreciable evolution of H₂ or O₂.⁵⁴ This result suggested that the increase in activity was attributable to interaction between Ni and Cr in the cocatalyst, motivating further investigation of Cr as a cocatalyst in combination with other transition metals.

We thus examined mixed transition metal oxides containing Cr as new cocatalysts for overall water splitting on GaN:ZnO.^{55–59} In a typical preparation, a coimpregnation method

was performed by suspending 0.3–0.4 g of GaN:ZnO powder in an aqueous solution containing an appropriate amount of Cr(NO₃)₃·9H₂O and the nitrate (or chloride) of the paired metal. The solution was then evaporated to dryness over a water bath followed by calcination in air at 623 K for 1 h. In the case of Ni or Ni–Cr cocatalysts, the impregnated material was reduced by exposure to H₂ (20 kPa) at 573 K for 2 h then oxidized by exposure to O₂ (10 kPa) at 473 K for 1 h in a closed gas circulation system to produce a Ni/NiO (core/shell) structure.⁶⁰

As listed in Table 1, the photocatalytic activity of various transition-metal-loaded catalysts was markedly improved by coloaded with Cr. All of the examples except for the Ag–Cr system achieved stoichiometric evolution of H₂ and O₂ from pure water. It should be noted that even though loading with Fe, Co, Cu, Pd, or Ag alone did not activate GaN:ZnO for overall water splitting, coloaded with Cr and one of these inactive metal components resulted in measurable photocatalytic activity. Coloaded Cr probably facilitated charge transfer from the bulk GaN:ZnO to the cocatalyst, and/or promoted the creation of catalytic gas-evolution sites on the cocatalyst surface. The largest improvement in activity was obtained by loading GaN:ZnO with a combination of 1.0 wt % Rh and 1.5 wt % Cr. The activity of this catalyst system was two orders of magnitude higher than for catalysts loaded with 1.0 wt % Rh under the same reaction conditions.

The photocatalytic activity of GaN:ZnO loaded with Cr and Rh was also found to be dependent on the calcination temperature after impregnation. The sample prepared without calcination did not produce H₂ or O₂. The rates of H₂ and O₂ evolution increased significantly with increasing calcination temperature to a maximum at 623 K, beyond which the activity of the samples began to decrease. The structural changes undergone by the catalyst in the various treatment steps were investigated by scanning electron microscopy (SEM), transmission electron microscopy (TEM), energy-dispersive X-ray analysis (EDX), X-ray photoelectron spectroscopy (XPS), and

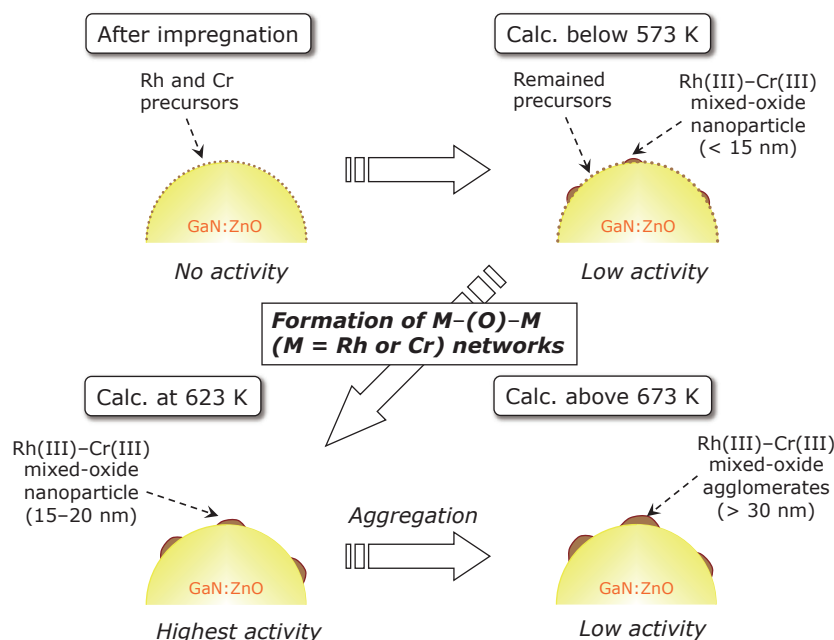


Figure 9. Structural changes undergone by GaN:ZnO modified with Rh and Cr species in the various treatment steps, which were investigated by SEM, TEM, EDX, XPS, and XAFS. Reproduced from ref 57 with permission. Copyright 2006 American Chemical Society.

X-ray absorption fine-structure spectroscopy (XAFS), and are depicted schematically in Figure 9. The results indicated that the activity of GaN:ZnO modified with Rh and Cr species is strongly dependent on the generation of trivalent Rh–Cr mixed oxide ($\text{Rh}_{2-y}\text{Cr}_y\text{O}_3$) nanoparticles (10–30 nm in size) with optimal composition and distribution.⁵⁷

3.2 Unique Properties of $\text{Rh}_{2-y}\text{Cr}_y\text{O}_3$ as a Cocatalyst.

The performance of $\text{Rh}_{2-y}\text{Cr}_y\text{O}_3$ -loaded GaN:ZnO for overall water splitting was an order of magnitude higher than that obtained by the previously optimized catalyst consisting of a conventional RuO_2 cocatalyst.⁵⁵ Results of photocatalytic reactions using sacrificial reagents (i.e., methanol and silver nitrate) indicated that the $\text{Rh}_{2-y}\text{Cr}_y\text{O}_3$ cocatalyst loaded on GaN:ZnO functioned not as an O_2 evolution site but rather as a H_2 evolution site, and that it was more efficient than RuO_2 . Considering the inactivity of bare GaN:ZnO for H_2 evolution and appreciable activity for O_2 evolution in the presence of sacrificial reagents, the relatively slow step for overall water splitting on GaN:ZnO is considered to be the water reduction process. Therefore, one of the reasons for the improvement in photocatalytic activity achieved by modification of GaN:ZnO with $\text{Rh}_{2-y}\text{Cr}_y\text{O}_3$ is the promotion of the H_2 evolution reaction, that is, an increase in the activity of the rate-determining step for overall water splitting. This is consistent with the results of photocatalytic H_2 and O_2 half reactions using different GaN:ZnO samples.⁵³

It is known that gaseous O_2 can suppress water splitting over a photocatalyst, as exemplified by NiO-loaded SrTiO_3 (ref 60), Pt-loaded TiO_2 (ref 61), and ZrO_2 (ref 62). This is because O_2 molecules can act as electron acceptors that react with photogenerated electrons in the conduction band of a photocatalyst. The thus-reduced O_2 species (e.g., $\bullet\text{O}_2^-$) are presumably oxidized by the valence band holes, thereby lowering the utilization efficiency of photogenerated charge carriers for

water splitting. This phenomenon is known as photoreduction of O_2 . We found that RuO_2 -loaded GaN:ZnO reductively reacted with O_2 , thereby lowering the rate of H_2 evolution. Interestingly, however, O_2 photoreduction on $\text{Rh}_{2-y}\text{Cr}_y\text{O}_3$ -loaded GaN:ZnO was negligibly slow, which should contribute to the higher activity of the $\text{Rh}_{2-y}\text{Cr}_y\text{O}_3$ -loaded sample than that of the RuO_2 sample.⁵⁶ The inertness of $\text{Rh}_{2-y}\text{Cr}_y\text{O}_3$ -loaded GaN:ZnO for the photoreduction of O_2 also suggests that the photocatalyst is suitable for use at atmospheric pressure. In fact, gas evolution from the reactant suspension dispersed with $\text{Rh}_{2-y}\text{Cr}_y\text{O}_3$ -loaded GaN:ZnO powder was observable as continuous bubbles at atmospheric pressure under irradiation by a high-pressure mercury lamp via Pyrex glass.⁵⁵ This is a very useful property for the purpose of practical applications.

The O_2 -insensitive character of $\text{Rh}_{2-y}\text{Cr}_y\text{O}_3/\text{GaN:ZnO}$ (more specifically $\text{Rh}_{2-y}\text{Cr}_y\text{O}_3$ nanoparticles) in turn implies high selectivity for H_2 evolution. In fact, $\text{Rh}_{2-y}\text{Cr}_y\text{O}_3/\text{GaN:ZnO}$ produced H_2 and O_2 from an aqueous solution containing NO_3^- ions,⁶³ which are more susceptible to reduction than protons ($\text{NO}_3^-/\text{NO}_2^-$, +0.40 V; H^+/H_2 , -0.41 V vs. NHE at pH 7). Stable H_2 evolution was also achieved using $\text{Rh}_{2-y}\text{Cr}_y\text{O}_3/\text{GaN:ZnO}$ in an aqueous solution containing I^- ions as electron acceptors.⁵³ IO_3^- ions, produced as the oxidation product of I^- , have been reported to prevent the reduction of H^+ (i.e., H_2 evolution) by reducing ahead of H^+ .^{64,65} This behavior is exemplified by the gradual decrease in the rate of H_2 evolution on Pt-loaded anatase TiO_2 (ref 64) and TaON powder⁶⁵ from an aqueous NaI solution as the reaction progresses. The stable behavior of $\text{Rh}_{2-y}\text{Cr}_y\text{O}_3/\text{GaN:ZnO}$ for H_2 evolution in the presence of IO_3^- is another indication of high selectivity of $\text{Rh}_{2-y}\text{Cr}_y\text{O}_3$ for H_2 evolution. $\text{Rh}_{2-y}\text{Cr}_y\text{O}_3/\text{GaN:ZnO}$ was also demonstrated to split seawater to produce H_2 and O_2 under visible light. More details on the photocatalytic activities of $\text{Rh}_{2-y}\text{Cr}_y\text{O}_3$ and RuO_2 -loaded ones, including the

effects of electrolyte in the reactant solution, are described elsewhere.⁶³

The optimized $\text{Rh}_{2-y}\text{Cr}_y\text{O}_3/\text{GaN}:\text{ZnO}$ achieved an AQY of ca. 5.1% at 410 nm for overall water splitting,¹⁷ at least an order of magnitude greater than that achieved using a RuO_2 -loaded analogue. The higher activity of $\text{Rh}_{2-y}\text{Cr}_y\text{O}_3/\text{GaN}:\text{ZnO}$ is a result of both the superior ability of $\text{Rh}_{2-y}\text{Cr}_y\text{O}_3$ nanoparticles to host H_2 evolution sites and the inactivity for O_2 photoreduction and H_2 - O_2 recombination, which are undesirable backward reactions that can occur during photocatalytic water splitting. The rate of visible-light water splitting over $\text{Rh}_{2-y}\text{Cr}_y\text{O}_3/\text{GaN}:\text{ZnO}$ was demonstrated to remain unchanged for 3 months (2160 h), producing H_2 and O_2 continuously in a stoichiometric amount, although after 6 months of operation, a 50% loss of the initial activity occurred.⁶⁶ Importantly, this $\text{Rh}_{2-y}\text{Cr}_y\text{O}_3$ cocatalyst is also applicable to other photocatalytic systems, such as TiO_2 , Ga_2O_3 , GaN, and $\text{ZnO}-\text{ZnGeN}_2$ solid solutions, to significantly enhance their photocatalytic water-splitting rates, regardless of the electronic configuration or the type of photocatalyst.^{23,58,67,68} By an in situ photodeposition method using $(\text{NH}_4)_3\text{RhCl}_6$ and K_2CrO_4 as precursors under O_2 -free conditions, it is possible to modify not only GaN:ZnO but also various semiconductors with $\text{Rh}_{2-y}\text{Cr}_y\text{O}_3$.^{69,70} This demonstrates the first example of the photodeposition of a mixed metal oxide using photoactive semiconductors.

3.3 New Type of Cocatalysts: Core/Shell-Structured Nanoparticles Consisting of Metal or Metal Oxide as the Core and Cr_2O_3 as the Shell.

3.3.1 Initial Concept for Designing the Core/Shell-Structured Cocatalysts: Noble metals in general function as efficient cocatalysts for H_2 evolution due to their high exchange current density and low overvoltage for the H_2 evolution reaction. However, they also catalyze water formation from H_2 and O_2 (a backward reaction of overall water splitting), limiting their usefulness as cocatalysts for overall water splitting on a particulate photocatalyst.⁶

We believed that the reverse reaction would be suppressed if nanoparticulate noble metal cocatalysts could be coated by a shell, forming a core/shell-like configuration. More specifically, we expected that the access of H_2 and O_2 molecules to the noble metal core would be suppressed using a shell coating. As such a shell component, we turned our attention to Cr_2O_3 , which was reported to function as a catalyst for some hydrogen-related reactions (e.g., (de)hydration)^{71,72} and to be deposited through a photochemical reduction process from Cr(VI) species as the precursor. Photoreduction of Cr(VI) ions over a semiconductor photocatalyst has been reported by several researchers as a potential method for detoxification of Cr(VI) species in environmental water.⁷³ The thermodynamic potential for the reduction of Cr(VI) into Cr(III) is more positive than that for water reduction, meaning that reductive deposition of Cr(III) species onto noble metals is possible when a photocatalyst having band gap positions suitable for water splitting is employed.

Note here that during the study of overall water splitting by $\text{Rh}_{2-y}\text{Cr}_y\text{O}_3/\text{GaN}:\text{ZnO}$, we found that a small amount of residual Cr(VI) species in $\text{Rh}_{2-y}\text{Cr}_y\text{O}_3/\text{GaN}:\text{ZnO}$ initially dissolved in the reactant solution, which subsequently underwent photoreduction into Cr(III) species.⁵⁶ Because photoreduction

of Cr(VI) did not occur on the surface of GaN:ZnO, we concluded that photoreductive deposition of Cr(III) species occurred on $\text{Rh}_{2-y}\text{Cr}_y\text{O}_3$ nanoparticles. This experimental observation inspired us to develop core/shell-structured nanoparticles consisting of a noble metal as the core and Cr_2O_3 as the shell.

3.3.2 Preparation, Characterization, and Functionality of Noble-Metal/ Cr_2O_3 (Core/Shell) Nanoparticles: We prepared noble-metal/ Cr_2O_3 (core/shell) nanostructures on GaN:ZnO through a stepwise photodeposition under oxygen-free conditions.^{74,75} The scheme is shown in Figure 10A. First, noble-metal nanoparticles were deposited using a proper metal salt complex under band gap irradiation of GaN:ZnO ($\lambda > 400$ nm). The as-prepared noble-metal/GaN:ZnO sample was then

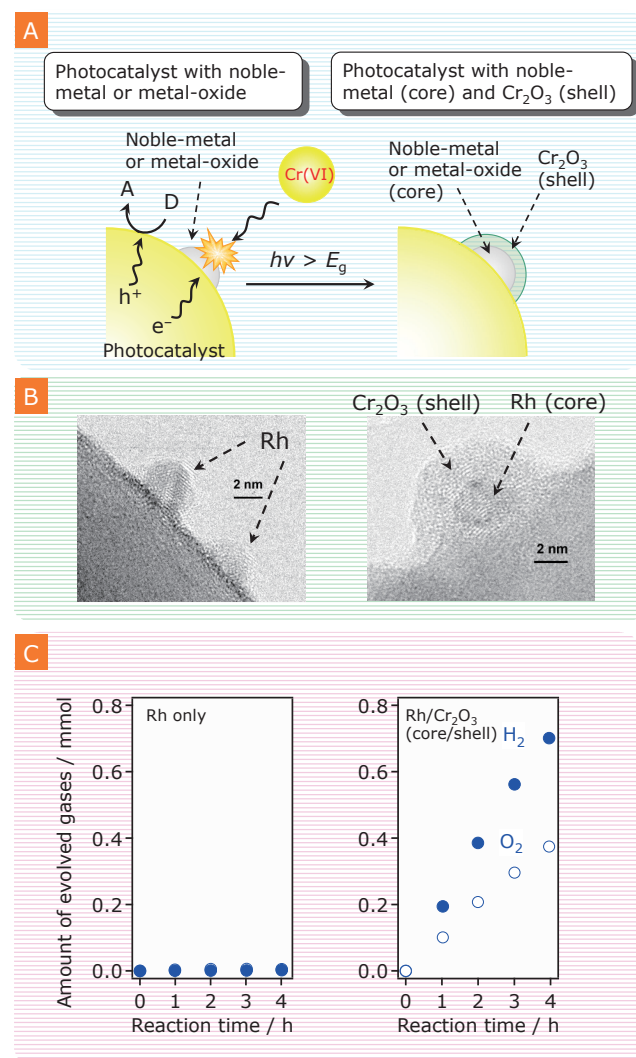


Figure 10. (A) Schematic illustration of Cr_2O_3 deposition through the reduction of Cr(VI) ions (D and A indicate electron donor and acceptor, respectively). (B) HR-TEM images of GaN:ZnO with photodeposited Rh (left) before and (right) after photodeposition of a Cr_2O_3 shell. (C) Time courses of overall water splitting under visible light ($\lambda > 400$ nm) using GaN:ZnO modified with (left) Rh and (right) core/shell-structured Rh/ Cr_2O_3 . Reproduced from ref 17 with permission. Copyright 2010 American Chemical Society.

treated with K_2CrO_4 in a similar manner. The final product was washed thoroughly with distilled water and dried overnight at 343 K.

TEM images of GaN:ZnO loaded with Rh nanoparticles followed by treatment with K_2CrO_4 and visible light are shown in Figure 10B. The primary particle size of the introduced Rh nanoparticles is 2–3 nm, with some aggregation to form larger secondary particles. On the other hand, the TEM images of the samples after K_2CrO_4 treatment show that the noble-metal nanoparticles are coated with a shell layer about 2 nm thick to form a core/shell nanostructure. It should be noted that the shell thickness is almost constant (ca. 2 nm), regardless of the kind of noble-metal nanoparticle or the size of such nanoparticles. Despite the fact that CrO_4^{2-} is a strong oxidizing reagent (i.e., it works as a strong electron acceptor), reduction of CrO_4^{2-} ions on GaN:ZnO did not occur due to the lack of adsorption sites.⁷⁵ This allows for the selective reduction of CrO_4^{2-} ions on Rh, which acts as an electron sink, resulting in the successful preparation of Rh/ Cr_2O_3 (core/shell) nanoparticles on GaN:ZnO. In the case of Rh as the core, it was confirmed by XAFS and XPS that the core and the shell consist of metallic Rh and Cr_2O_3 , respectively.

Figure 10C shows time courses of water splitting using some GaN:ZnO samples under visible light ($\lambda > 400$ nm). Rh-loaded GaN:ZnO exhibited little photocatalytic activity for overall water splitting even for extended periods of irradiation, most likely due to rapid water formation on Rh nanoparticles. However, GaN:ZnO loaded with the Rh-core/ Cr_2O_3 -shell nanoparticles exhibited stoichiometric H_2 and O_2 evolution from pure water, indicating the occurrence of overall water splitting. Addition of the Rh-loaded sample to the reactant suspension containing the Rh/ Cr_2O_3 -loaded one, however, resulted in a marked decrease in the rates of both H_2 and O_2 evolution. It is thus clear that water formation from H_2 and O_2 on unmodified Rh nanoparticles occurs rapidly in the overall water-splitting reaction, and that the suppression of water formation is essential for achieving efficient evolution of H_2 and O_2 in this system. It was confirmed that the use of other noble metals, such as Pd and Pt, as a core with the Cr_2O_3 shell in the same manner achieved the same function as observed here for Rh.

The thickness of the Cr_2O_3 shell deposited on the noble metal core could be controlled by changing the initial concentration of K_2CrO_4 in the preparation process, although precise control remained a challenge.⁷⁵ With increasing the K_2CrO_4 concentration, the thickness of the Cr_2O_3 shell became thicker and more homogeneous. After the thickness reached ca. 2 nm, further shell deposition did not occur. The growth of the Cr_2O_3 shell contributed directly to enhancement of the water-splitting rate. The Cr_2O_3 shell thickness was also dependent on the pH of the solution in which the photoreduction of K_2CrO_4 was conducted.⁷⁶ As a result, the water-splitting activity of samples prepared at different pHs varied. When the deposition pH ranged from 3.0 to 7.5, there was almost no change in activity, with stoichiometric evolution of H_2 and O_2 under visible light. As the pH decreased from 3.0 to 2.0, however, the rates of H_2 and O_2 evolution both decreased significantly. TEM observations showed that, in the Rh-photodeposited GaN:ZnO treated with K_2CrO_4 and visible light at pH 2.0, almost no shell forma-

tion could be identified, in contrast to the sample treated at pH 7.5. At pH below 3.0, the photoreduction of Cr(VI) ions occurred. At this pH condition, the Cr(III) ions could not precipitate as Cr(III) hydroxide or oxide. It is therefore concluded that a relatively neutral pH is a better choice when coating nanoparticulate cores with Cr_2O_3 shells.

It is very important to understand the reaction mechanism at a molecular scale in order to design more efficient photocatalytic systems. The mechanism of H_2 evolution on core/shell-structured nanoparticles was therefore investigated using electrochemical and in situ spectroscopic measurements of model electrodes that consisted of Rh and Pt plates with electrochemically deposited 1.8- to 3.5-nm-thick Cr_2O_3 .⁷⁷ For both Cr_2O_3 -coated and bare electrodes, proton adsorption/desorption and H_2 evolution currents were observed, and an infrared absorption band assigned to Pt–H stretching was apparent. Therefore, the Cr_2O_3 layer did not interfere with proton reduction or H_2 evolution, and proton reduction took place at the Cr_2O_3 /Pt interface, different from our initial expectations as mentioned above. However, the reduction of oxygen was suppressed only in the Cr_2O_3 -coated samples. It was concluded that the Cr_2O_3 layer was permeable to protons and evolved H_2 molecules, but not to oxygen. The reaction mechanism of H_2 evolution on core/shell-structured nanoparticles (with a noble metal or metal oxide core and a Cr_2O_3 shell) in photocatalytic overall water splitting is illustrated in Figure 11.

Another noticeable feature of this Rh/ Cr_2O_3 (core/shell) system is that Cr_2O_3 shell deposition only occurs up to a thickness of ca. 2 nm, and is independent of the Rh core size.^{74,75} The reason for the inhibition of CrO_4^{2-} reduction onto Cr_2O_3 shells of more than 2 nm in thickness still remains unclear, and the detailed mechanism by which the Cr_2O_3 shell is formed is complex and needs further investigation. One possible explanation for the self-limiting nature of the Cr_2O_3 shell formation is the difference in reduction processes between Cr(VI)/Cr(III) and H^+/H_2 . It appears that the photoreduction of Cr(VI) into

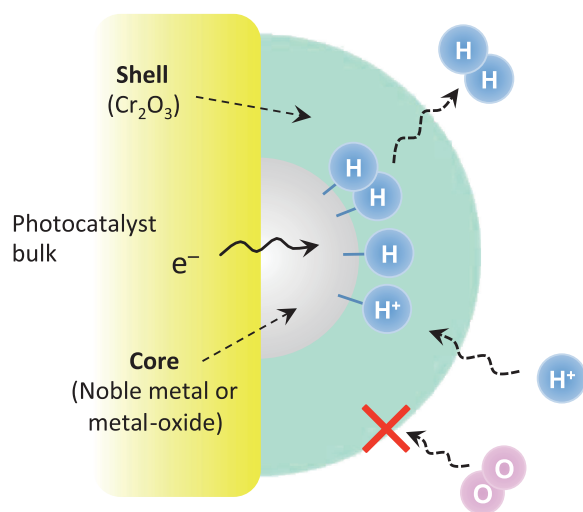


Figure 11. Reaction mechanism of H_2 evolution on core/shell-structured nanoparticles (with a noble metal or metal oxide core and a Cr_2O_3 shell) in photocatalytic overall water splitting. Reproduced from ref 17 with permission. Copyright 2010 American Chemical Society.

Cr(III) involving a complex 3-electron redox process⁷⁸ is more difficult than kinetically simpler processes, such as H^+ reduction. It has been reported by Bard et al. that electron tunneling can take place across an electrochemically passivated oxide layer with a thickness of 0.5–2.5 nm on a Cr electrode, and the tunneling electron transfer is hindered with increasing thickness of the passivated oxide layer.⁷⁹ The same tendency was observed in the Rh/Cr₂O₃ model electrode system.⁷⁷ It is therefore considered that the present electron penetration through the Cr₂O₃ shell is due to such a tunneling electron-transfer phenomenon, but the efficiency of electron transfer from the Rh core to the external surface of the Cr₂O₃ shell decreases with increasing thickness of the Cr₂O₃ shell. As a result, with increasing thickness of the Cr₂O₃ shell, the reduction of CrO₄²⁻ into Cr₂O₃ involving 3-electron transfer is more difficult. Finally, when the thickness of the Cr₂O₃ shell reaches about 2 nm, the reduction of CrO₄²⁻ ceases and the H₂ evolution as a result of H⁺ reduction proceeds preferentially.

3.3.3 Size Effect of the Core: Among the noble metals examined as the core component, Rh was the most effective for enhancing activity of GaN:ZnO for overall water splitting under visible light. However, in the original preparation method, the Rh-core nanoparticles tended to aggregate on the catalyst.⁷⁴ Because the activity of a heterogeneous catalytic system is generally dependent on the surface area available for reaction, the activity of the Rh-core/Cr₂O₃-shell system should be enhanced further if aggregation of the cocatalyst nanoparticles can be prevented. Therefore, increasing the dispersion of cocatalysts in a given system is a reasonable strategy for improving the photocatalytic activity.

Highly dispersed Rh nanoparticles were successfully loaded on GaN:ZnO without aggregation by adsorbing Rh nanoparticles that were protected by 3-mercaptopropylsulfonic acid or poly(*N*-vinyl-2-pyrrolidone), followed by calcination under vacuum or air at 673 K.^{80,81} After the Rh nanoparticles were coated with a Cr₂O₃-shell, the photocatalytic activity for overall water splitting was tested under visible-light irradiation. As expected, the sample with a better dispersion of Rh, which was prepared using 3-mercaptopropylsulfonic acid and had an average size of 1.9 ± 0.6 nm, exhibited activity much higher than an analogue containing poorly dispersed Rh nanoparticles prepared by a photodeposition method.⁸⁰ Photocatalytic activity of this Rh-core/Cr₂O₃-shell system for overall water splitting was further investigated with respect to the size of the Rh core using Rh nanoparticles that had sizes of 1.5–6.6 nm and narrow size distribution.⁸¹ The result showed that the photocatalytic activity was improved by decreasing the size of Rh nanoparticles, and the highest activity was obtained when 1.5 nm Rh nanoparticles were deposited without aggregation. According to a similar concept, Negishi and Kudo et al. reported that highly dispersed ca. 1 nm Au nanoclusters served as efficient cocatalysts for H₂ evolution, thereby promoting overall water splitting by BaLa₄Ti₄O₁₅ under UV irradiation ($\lambda > 200$ nm).⁸²

3.3.4 Application to Cr₂O₃ Modification to Metal Oxide Core Systems: It was thus demonstrated that the “core/shell” strategy is promising for noble-metal/photocatalyst systems to allow for H₂ and O₂ evolution from water, because backward reactions involving molecular O₂ (e.g., H₂–O₂ recombination)

are effectively suppressed by the Cr₂O₃ shell surrounding the noble metals. Although this functionality is essential for a noble-metal-loaded photocatalyst to achieve overall water splitting, it is not necessarily required for a metal oxide-loaded one because metal oxide cocatalysts generally exhibit negligible catalytic activity for water formation. In some cases, however, metal oxide cocatalysts undergo degradation due to a change in the cocatalyst state by exposure to the reactant solution, and catalyze O₂ photoreduction (another backward reaction of water splitting), which leads to a decrease in activity, as exemplified by GaN:ZnO modified with RuO₂ (ref 56) or CuO.⁵⁹

When the loaded metal oxide nanoparticles are covered with Cr₂O₃, this deactivation and O₂ photoreduction should be suppressed by a reduced accessibility of the loaded metal oxides to the reactants. This idea stimulated our investigation of the activity of a metal oxide-loaded photocatalyst modified with Cr₂O₃ photodeposits for overall water splitting. The effectiveness of Cr₂O₃ modification toward the enhancement of the water-splitting rate was highlighted using GaN:ZnO modified with three different metal oxides of NiO_x, Rh₂O₃, and RuO₂.⁷⁶ It has been pointed out that the activity of a NiO_x-loaded photocatalyst for overall water splitting can be degraded in some cases, due to the hydrolysis of NiO_x into Ni(OH)₂ and/or peeling off.²⁰ In fact, the rates of H₂ and O₂ evolution over NiO_x-loaded GaN:ZnO decreased with reaction time. Interestingly, however, modification of NiO_x/GaN:ZnO with Cr₂O₃ resulted in enhanced, stable H₂ and O₂ evolution. In the case of Rh₂O₃ cocatalyst, while the deposition of this cocatalyst onto GaN:ZnO did not yield any activity for water splitting, Cr₂O₃/Rh₂O₃/GaN:ZnO produced appreciable amounts of H₂ and O₂ in a stoichiometric ratio. In these two cases, uniform deposition of the Cr₂O₃ shell, as observed in noble-metal/Cr₂O₃ systems, was not observed.

A similar activity enhancement was also observed for Cr₂O₃-modified RuO₂-loaded GaN:ZnO. As discussed earlier, RuO₂/GaN:ZnO was demonstrated to catalyze O₂ photoreduction, and RuO₂ was supposed to work as a H₂ evolution site on GaN:ZnO.⁵⁶ If all of the RuO₂ nanoparticles on GaN:ZnO function as electron collectors, Cr₂O₃ should coat all of them without exception. However, this was not the case; some of the RuO₂ nanoparticles remained uncovered even after visible-light irradiation in the presence of excess K₂CrO₄. Surprisingly, an intentional addition of O₂ gas into the reaction system with Cr₂O₃/RuO₂/GaN:ZnO did not reduce the rate of H₂ evolution, while the H₂ evolution over RuO₂/GaN:ZnO decreased significantly. RuO₂ is an interesting cocatalyst that can promote both reduction and oxidation photocatalysis, although its performance as a water-splitting photocatalyst is moderate.⁵⁶ In the present case, it appears that the uncoated RuO₂ nanoparticles on GaN:ZnO work as hole trap sites to promote water oxidation.

Thus, photodeposition of Cr₂O₃ was shown to be an effective approach to improve the activity for overall water splitting under visible light. It is likely that suppressing undesirable chemical changes of a cocatalyst and/or O₂ photoreduction contributed to this enhanced photocatalytic activity. Therefore, Cr₂O₃ photodeposition can improve H₂ evolution, not only on noble metals but also on metal oxides. Another core/shell cocatalyst for photocatalytic overall water splitting, Ni-core/NiO-shell nanoparticles, has been applied to many heteroge-

neous photocatalytic systems.^{15,19,22,60} Compared with Ni/NiO, the present noble metal (or metal oxide)/Cr₂O₃ core/shell cocatalyst has several advantages, including (1) the possibility of using various noble metals and metal oxides as a core for the extraction of photogenerated electrons from the photocatalyst bulk, (2) the possibility of selectively introducing active species for overall water splitting at reduction sites on the photocatalyst, and (3) elimination of the need for activation treatment by oxidation or reduction. The latter two advantages are effective when the core is introduced by an in situ photodeposition method (although it may involve another problem of aggregation of metal deposits). The elimination of activation procedures involving heat treatment is especially beneficial for non-oxide photocatalysts, which have inherent instability toward heat-treatment.

3.4 Coloading of Reduction and Oxidation Cocatalysts for Overall Water Splitting. As discussed above, significant efforts have been made toward the development of an efficient water reduction cocatalyst. Here, it would be natural to expect that loading both H₂ and O₂ evolution cocatalysts onto the same photocatalyst would improve water-splitting activity, compared to photocatalysts modified with either an H₂ or O₂ evolution cocatalyst. However, the actual demonstration of this remained a challenge.

We demonstrated a proof-of-concept using GaN:ZnO loaded with Rh/Cr₂O₃ (core/shell) and Mn₃O₄ nanoparticles as H₂ and O₂ evolution promoters, respectively, under visible light.⁸³ The preparation scheme is shown in Figure 12A. First, Mn oxide was introduced onto GaN:ZnO as an O₂ evolution cocatalyst. Some Mn oxides have been reported to serve as O₂ evolution

promoters,⁸⁴ and it is well known that the O₂ evolution center in the photosynthesis of green plants contains a Mn complex.⁸⁵ MnO nanoparticles with a mean size of 9.2 ± 0.4 nm were adsorbed onto GaN:ZnO. The as-prepared MnO/GaN:ZnO sample was then calcined in air at 673 K for 3 h to remove organic residues that served as stabilizers of MnO nanoparticles. With this calcination treatment, MnO nanoparticles transformed into Mn₃O₄, but the particle size of the Mn oxide was maintained. Thus, GaN:ZnO particles were successfully decorated with Mn₃O₄ nanoparticles. As expected, PEC measurements indicated that the loaded nanoparticles of Mn₃O₄ functioned as O₂ evolution sites. On the other hand, Mn₃O₄/GaN:ZnO did not promote H₂ evolution from an aqueous solution containing methanol as an electron donor, indicating that Mn₃O₄ on GaN:ZnO does not host water reduction sites.

Next, core/shell-structured Rh/Cr₂O₃ nanoparticles were introduced as H₂ evolution sites into Mn₃O₄-loaded GaN:ZnO by an in situ photodeposition method that in principle allows for the deposition of metal nanoparticles on the reduction sites of a given photocatalyst.⁸⁶ TEM observation with EDX analysis revealed that Rh/Cr₂O₃ (core/shell) and Mn₃O₄ nanoparticles were separately loaded on the GaN:ZnO, although part of the Rh cores were aggregated⁷⁴ and there was little EDS signal of Rh on the Mn₃O₄ nanoparticles. We thus concluded that Rh/Cr₂O₃ (core/shell) nanoparticles were successfully introduced onto Mn₃O₄/GaN:ZnO without concealing the pre-deposited Mn₃O₄ nanoparticles and changing the original size of 9–10 nm.

As mentioned above, GaN:ZnO modified with core/shell-structured Rh/Cr₂O₃ nanoparticles catalyzed overall water splitting steadily. In contrast, Mn₃O₄/GaN:ZnO did not pro-

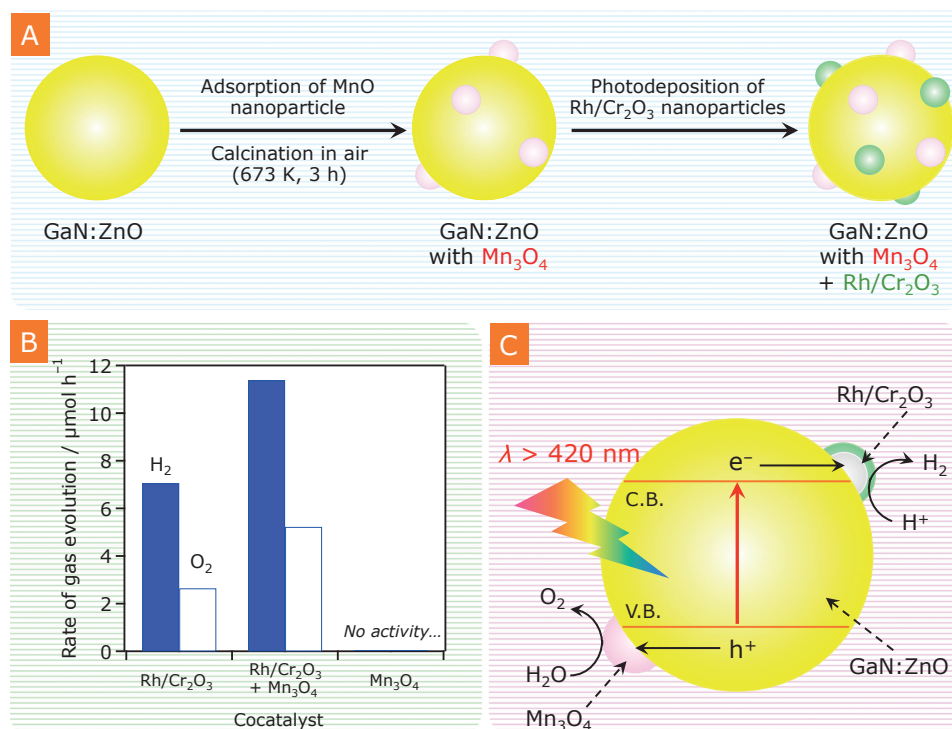


Figure 12. (A) Scheme for the preparation of GaN:ZnO loaded with both Mn₃O₄ and core/shell-structured Rh/Cr₂O₃. (B) Photocatalytic activity of GaN:ZnO modified with different cocatalysts under visible light ($\lambda > 420$ nm). (C) Illustration of the reaction scheme for overall water splitting on GaN:ZnO modified with Mn₃O₄ and core/shell-structured Rh/Cr₂O₃. Reproduced from ref 17 with permission. Copyright 2010 American Chemical Society.

duce any H₂ or O₂, again indicating the necessity of loading H₂ evolution sites on GaN:ZnO to achieve overall water splitting. Interestingly, GaN:ZnO modified with both Rh/Cr₂O₃ and Mn₃O₄ exhibited enhanced activity, compared to catalysts modified with either Rh/Cr₂O₃ or Mn₃O₄ (Figure 12B). The photocatalytic activity was also found to be dependent on the loading amount of Mn₃O₄. The rates of H₂ and O₂ evolution both increased with increasing Mn loading, reaching a maximum at 0.05 wt%, beyond which the activity began to decrease.

On the basis of the above results, a reaction mechanism for visible-light-driven overall water splitting on this catalyst can be proposed (Figure 12C). The loaded Mn₃O₄ nanoparticles function as O₂ evolution cocatalysts, as indicated by PEC measurements, while Rh/Cr₂O₃ (core/shell) nanoparticles serve as H₂ evolution sites. With the aid of nanoparticulate Mn₃O₄ in O₂ evolution, the photocatalytic activity for overall water splitting by GaN:ZnO modified with core/shell-structured Rh/Cr₂O₃ nanoparticles was improved compared to analogues modified with either H₂ or O₂ evolution cocatalysts. Similar enhancement of activity was observed when other metal oxides, which are reported to work as water oxidation promoters, were loaded, indicating the general adoptability of this concept.⁸⁷ These results are in good agreement with our kinetic assessment of overall water splitting using GaN:ZnO modified with Rh–Cr mixed oxide as an H₂ evolution cocatalyst, which suggests that there is room for improvement of water-splitting activity by introducing suitable O₂ evolution sites in addition to H₂ evolution sites.⁸⁸ It was also demonstrated that the present coloaded method was applicable to a metal oxide photocatalyst such as SrTiO₃, suggestive of the general utility of this method. In addition to the overall water-splitting reaction, the coloaded method enabled us to improve the water-oxidation half reaction over WO₃ in the presence of a reversible electron acceptor.⁸⁹

4. Activation of (Oxy)nitrides with d⁰ Electronic Configurations

4.1 Early Works on d⁰-(Oxy)nitrides. As discussed, the findings of GaN:ZnO solid solutions and new types of cocatalysts allowed us to achieve overall water splitting under visible light. However, the longest wavelength available for overall water splitting using GaN:ZnO was at most 500 nm. For efficient solar energy conversion, a photocatalyst that harvests visible light at wavelengths longer than 600 nm (band gap smaller than 2.0 eV) is highly desirable.¹⁷ Assuming overall water splitting with a QY of unity, the theoretical potential of photocatalysts with a 500 nm absorption edge is 7.9% solar-energy-conversion efficiency, while photocatalysts with an absorption edge of 600 and 650 nm can, respectively, achieve 16.2 and 20.6% efficiencies.¹⁷ Thus, the development of photocatalysts that are capable of harvesting a wider range of visible light is an important subject for solar energy conversion.

d⁰-type (oxy)nitrides are more advantageous than d¹⁰-ones in terms of their light-absorption properties. However, direct splitting of pure water using d⁰-(oxy)nitrides remains a challenge. Alternatively, some d⁰-(oxy)nitrides work as building blocks for H₂ and/or O₂ evolution in a Z-scheme water-splitting system, which is another approach to achieve water splitting with visible light, and was originally introduced by Bard in

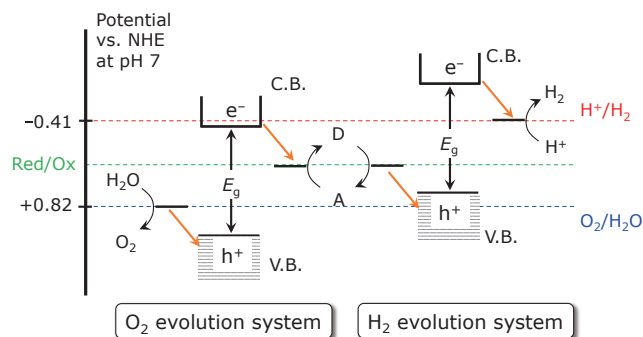
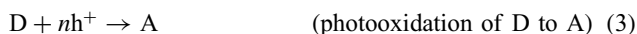
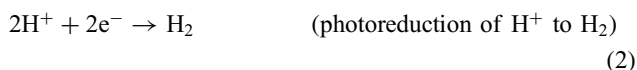
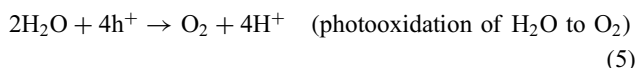
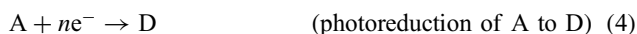


Figure 13. Schematic energy diagrams of photocatalytic water splitting for a two-step photoexcitation system. D and A indicate electron donating and accepting species, respectively. Reproduced from ref 91 with permission.

1979.⁹⁰ This system was inspired by natural photosynthesis in green plants, where photosystems I and II harvest 700 and 680 nm photons, respectively, oxidizing H₂O into O₂ under sunlight, with a QY close to unity. In this system, two different photocatalysts are combined using an appropriate shuttle redox mediator, as shown in Figure 13. Visible light can be utilized more efficiently than in the conventional one-step water-splitting systems because the energy required to drive each photocatalyst is reduced. It is also possible to apply a photocatalyst that has either water reduction or oxidation potential to one side of the system. For example, WO₃, which is unable to reduce H⁺, but able to produce O₂ from an aqueous solution containing appropriate electron acceptors under visible light, works as an effective building block for O₂ evolution in Z-scheme water splitting.^{4,5,9} In the H₂ evolution system, the forward reactions that should occur on the photocatalyst surface are the reduction of protons by conduction band electrons and the oxidation of an electron donor (D) by valence band holes to yield the corresponding electron acceptor species (A), as follows:



On the other hand, the forward reactions on an O₂ evolution photocatalyst are as follows:



where the electron acceptor generated by the paired H₂ evolution photocatalyst is converted to its reduced form (D), and water oxidation occurs with the valence band holes. Thus, the redox pair (D and A) is cycled, and the water-splitting reaction is achieved.

In 2005, Abe et al. applied Pt-loaded TaON as a H₂ evolution photocatalyst to a Z-scheme water-splitting system in combination with PtO_x/WO₃ as an O₂ evolution photocatalyst and an IO₃⁻/I⁻ redox mediator.⁶⁵ Further screening of (oxy)nitrides for application in H₂ evolution systems allowed the increase of the absorption wavelength available for H₂ evolution to 660 nm using BaTaO₂N.⁹² For more efficient utilization of visible photons in O₂ evolution, the replacement of WO₃ by

an (oxy)nitride with a longer absorption edge was realized using RuO₂/TaON that has absorption edges of 520 nm in the presence of an IO₃⁻/I⁻ redox mediator.⁹³ However, the efficiencies of these systems remained very low (at most AQY < 1%). Note that PtO_x/WO₃ is able to produce O₂ from an aqueous NaIO₃ solution under visible light, with an AQY of ca. 10%,⁸⁹ at least an order of magnitude higher than that of the total efficiency of the Z-scheme systems consisting of the material as the O₂ evolution building block. This means that the low efficiency of the oxynitride-based Z-scheme is due to the H₂ evolution system that consists of oxynitrides, which appears to be the main obstacle to achieving overall water splitting using these materials.

Thus, we needed to improve the H₂ evolution activities of (oxy)nitrides for both one-step and two-step water-splitting schemes. Even in the case of GaN:ZnO solid solutions that are capable of splitting pure water, it has been suggested that the rate-determining step for overall water splitting is the H₂ evolution process.⁵³ Several new modifications to enhance the H₂ evolution rate of d⁰-type (oxy)nitrides have thus been pursued as discussed in the following sections.

4.2 New Precursor Route for the Synthesis of Tantalum-Based (Oxy)nitrides. A straightforward way to activate a particulate photocatalyst would be to reduce the particle size, since a smaller particle size results in a shorter diffusion length for photogenerated electron–hole pairs in a given photocatalyst, reducing the recombination between electrons and holes and enhancing photocatalytic activity.^{3,6} Ta₃N₅ nanoparticles can be readily prepared by nitriding a nanoparticulate Ta₂O₅ precursor that is synthesized in advance through a precipitation method.⁹⁴ Compared to the conventional submicron-sized Ta₃N₅ particles, Ta₃N₅ nanoparticles with a smaller particle size of 30–50 nm exhibited enhanced photocatalytic activity for H₂ evolution from an aqueous methanol solution under visible light. UV–visible diffuse reflectance spectroscopy and PEC measurements suggested that the enhancement was due to the promotion of the water reduction process that originated from the lower defect density of the material, and that the particle size reduction was not the main reason in this particular case. Similar nanostructuring of Ta₃N₅ for enhanced H₂ evolution photocatalysis was realized using a mesoporous graphitic carbon nitride (mpg-C₃N₄) as a hard template. Ta₃N₅, having the smallest particle size that was prepared from mpg-C₃N₄ with a pore size of 7 nm, exhibited approximately one order of magnitude higher activity than bulk Ta₃N₅.⁹⁵

Using lamellar solids (RbCa₂Ta₃O₁₀ or HCa₂Ta₃O₁₀) as precursors, it is possible to synthesize CaTaO₂N particles having relatively low defect density. The as-prepared CaTaO₂N exhibited an enhanced activity for H₂ evolution from an aqueous methanol solution, compared to an analogue prepared from a conventional bulk type Ca–Ta oxide.⁹⁶

4.3 Surface Modification of TaON with ZrO₂ Nanoparticles.

4.3.1 Initial Concept: We also attempted to increase the photocatalytic activity of TaON for H₂ evolution under visible light by reducing the particle size. However, it was difficult to suppress the generation of defects during the nitridation process. As a result, the as-obtained TaON did not show an appreciable increase in photocatalytic activity, despite a rela-

tively small particle size (50–80 nm).⁹⁷ Although the calcination of solid photocatalysts at elevated temperatures after preparation has been demonstrated to be an effective approach for reducing the density of defects while maintaining the composition of the material,^{98–100} such post-calcination seemed to be disadvantageous for TaON due to its relatively low thermal stability. In fact, post-calcination of TaON under O₂ or N₂ results in a decrease in activity.¹⁰¹ The elimination of defects in TaON therefore remains a challenge.

To overcome such issues in the synthesis of TaON, we have developed a new strategy to reduce surface defects on TaON using ZrO₂ as a “protector” through a surface modification technique.¹⁰² Specifically, monoclinic ZrO₂ nanoparticles are dispersed on the surface of a Ta₂O₅ precursor before nitridation, thereby protecting Ta⁵⁺ cations in the TaON surface from being reduced by H₂ (derived from disassociation of NH₃ at high temperatures) during nitridation. The reduction of Ta⁵⁺ cations in TaON during nitridation generates reduced tantalum species, resulting in the production of anionic vacancies to maintain the charge balance of the material. The thus-formed defect sites can serve as recombination centers between photogenerated electrons and holes, resulting in an activity drop. On the other hand, when ZrO₂, more resistant to thermal ammonolysis than Ta₂O₅, is loaded on the surface of Ta₂O₅, Ta⁵⁺ cations at the interface between Ta₂O₅ (and/or TaON) and the loaded ZrO₂ are expected to interact with ZrO₂ and thereby become less sensitive to reduction. As a result, the undesirable reduction of Ta⁵⁺ cations during nitridation is suppressed. The above-mentioned idea and the preparation scheme are shown in Figure 14. Note that under visible-light irradiation ($\lambda > 400$ nm), the ZrO₂ modifiers do not involve any photoinduced electron-transfer events, because the band gap of ZrO₂ (ca. 5 eV) is too large to harvest >400 nm light and the CBM and VBM straddle those of TaON. In other words, surface photochemical reactions take place on the surface of the TaON component in the ZrO₂/TaON composite photocatalyst.

4.3.2 Preparation and Characterization: ZrO₂/TaON composites were prepared by heating ZrO₂-loaded Ta₂O₅ under a flow of NH₃ at 1123 K according to the preparation scheme in Figure 14. The as-prepared material was confirmed by XRD, SEM, and TEM to be a composite of monoclinic ZrO₂ and TaON, and the loaded ZrO₂ species existed on the TaON component in the form of nanoparticles (10–30 nm in size).^{102,103} With increasing ZrO₂ content, the ZrO₂ modifiers tended to aggregate.

Figure 15A shows UV–visible diffuse reflectance spectra of TaON and ZrO₂/TaON. The absorption band edge of TaON at ca. 520 nm, which is due to electron transition from the valence band formed by the hybridization of N2p and O2p orbitals to the conduction band consisting of empty Ta5d orbitals, remained almost unchanged even upon ZrO₂ modification. However, ZrO₂/TaON displayed a lower absorption band in the longer wavelength region, which is derived from reduced tantalum species (e.g., Ta³⁺ and Ta⁴⁺), as compared to unmodified TaON. This result indicates that ZrO₂ modification is effective for suppressing the formation of reduced tantalum species (i.e., defect sites) during nitridation. The as-prepared TaON powder is yellowish-green in color, while the ZrO₂/TaON composite is brilliant yellow (Figure 15B).

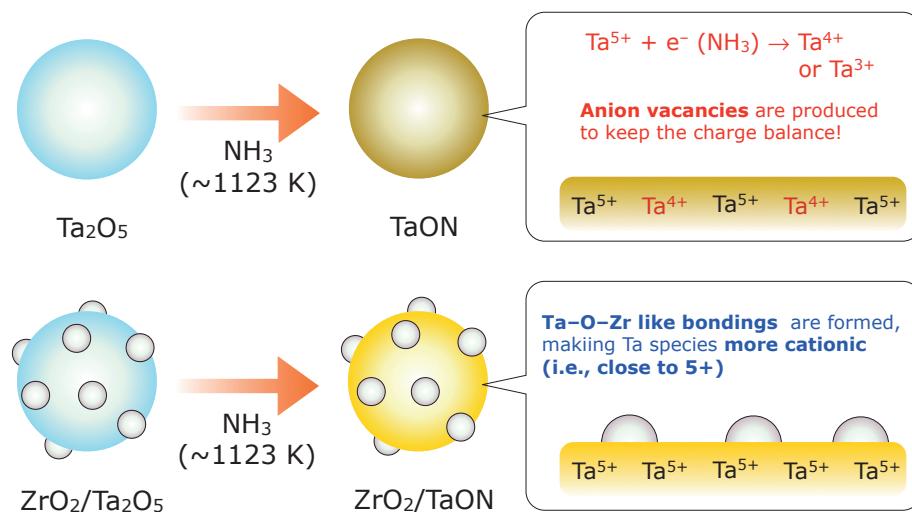


Figure 14. Nitridation of the $\text{ZrO}_2/\text{Ta}_2\text{O}_5$ composite to produce ZrO_2/TaON while suppressing the production of reduced tantalum species (defect sites) near the surface of the material. Reproduced from ref 10 with permission from the PCCP Owner Societies.

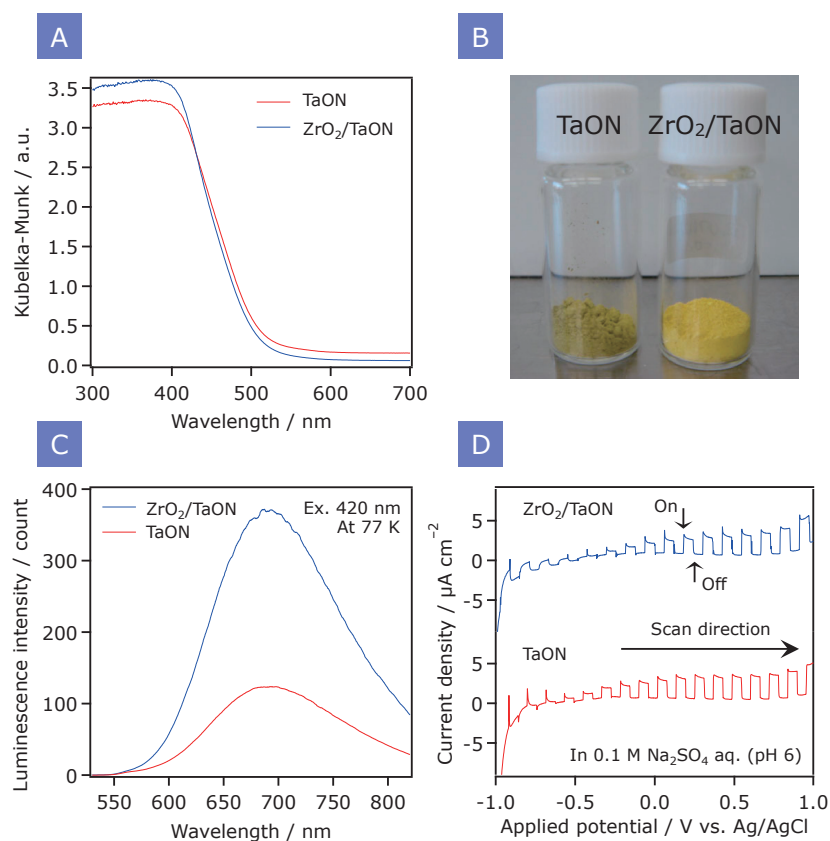


Figure 15. Comparison of ZrO_2/TaON ($\text{Zr}/\text{Ta} = 0.1$ by mole) with unmodified TaON. (A) UV-visible diffuse reflectance spectra, (B) digital photographs, (C) photoluminescence spectra, and (D) photoelectrochemical responses. Reproduced from ref 104 with permission. Copyright 2010 American Chemical Society.

The less-defective nature of the ZrO_2/TaON composite was also confirmed by photoluminescence spectroscopy.¹⁰⁴ As shown in Figure 15C, both TaON and ZrO_2/TaON exhibit a luminescence band centered at ca. 690 nm upon photoexcitation of 420 nm photons. However, the luminescence intensity of ZrO_2/TaON is ca. 3 times larger than that of TaON, even though the penetration of the incident photons is partially blocked by the ZrO_2 component that cannot be excited by

420 nm photons. This result could be explained in terms of the reduced density of nonradiative recombination sites in ZrO_2/TaON ; more specifically, donor levels, formed by the reduced Ta species, below the conduction band of TaON would act as effective traps of photogenerated carriers.

4.3.3 Photocatalytic Activity: Photocatalytic activity of ZrO_2/TaON was first evaluated using methanol as an electron donor under visible light with the aid of Ru nanoparticles. The

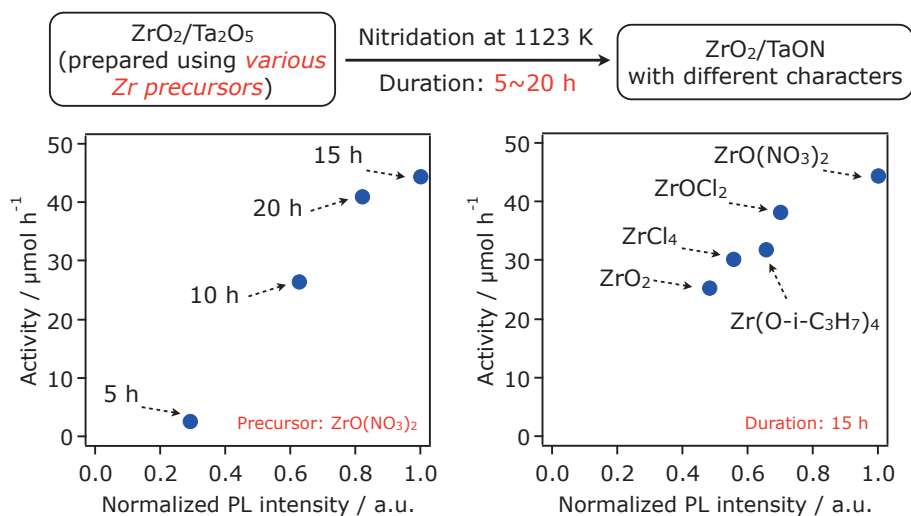


Figure 16. Relationship between the rate of H₂ evolution and photoluminescence intensity of ZrO₂/TaON catalysts synthesized (A) at different nitridation times with the same ZrO(NO₃)₂·2H₂O precursor and (B) from different Zr precursors with a common nitridation time of 15 h. Reproduced from ref 103 with permission from The Royal Society of Chemistry.

H₂ evolution activity from an aqueous methanol solution was increased upon an increase in the Zr/Ta ratio, reaching a maximum at Zr/Ta = 0.1, beyond which it began to decrease gradually. It is noted that regardless of the kind of cocatalysts loaded, an enhanced activity from an aqueous methanol solution was obtained with ZrO₂/TaON. It would be reasonable to conclude that the improvement in activity is attributable to the reduction of defects, while the activity drop observed in the higher Zr/Ta samples would be due to the excess coverage of ZrO₂, which blocks the active site for redox reactions on the TaON component and hinders absorption of the incident photons.

In order to develop guidelines for the preparation of a highly active photocatalyst, we investigated several factors affecting the photocatalytic activity of ZrO₂/TaON for H₂ production. ZrO₂/TaON (Zr/Ta = 0.1) photocatalysts were prepared by loading particulate Ta₂O₅ with ZrO₂ using different zirconium precursors (ZrO(NO₃)₂·2H₂O, ZrOCl₂·8H₂O, ZrCl₄, Zr(O-*i*-C₃H₇)₄, and ZrO₂), followed by nitridation at 1123 K for different durations (5–20 h) under NH₃ flow. Nitridation of ZrO₂/Ta₂O₅ for 15 h resulted in the production of ZrO₂/TaON, regardless of the zirconium precursors used, but the physicochemical properties varied. When changing the nitridation time from 5 to 20 h while using the same precursor (ZrO(NO₃)₂·2H₂O), a volcano-type relationship between nitridation time and activity was obtained. The highest activity was obtained for ZrO₂/TaON synthesized from Ta₂O₅ and ZrO(NO₃)₂·2H₂O after nitridation for 15 h. Note that the optimal sample contains highly dispersed ZrO₂ nanoparticles 10–30 nm in size on the surface of the TaON component.

Photoluminescence spectra of samples nitrided for different durations with various precursors were acquired. All samples exhibited a luminescence band at ca. 690 nm upon photoexcitation at 420 nm. However, the luminescence intensity differed, suggesting different densities of defect sites in these materials. Figure 16 shows the relationship between the luminescence intensity and activity of ZrO₂/TaON. It is clear that there is a linear relationship between the two factors, regardless

of precursors used and nitridation time. Based on these physicochemical analyses, we concluded that a lower density of anionic defects in TaON, which was realized using highly dispersed nanoparticulate ZrO₂, contributed primarily to the enhanced activity. Attempts have also been made to reduce the density of defects in a similar manner but with different elemental sources (e.g., Al and Si). However, none yielded higher performance than ZrO₂ modification.

Another interesting feature of ZrO₂/TaON is that this material exhibits both p- and n-type photoresponses (i.e., it behaves as an intrinsic semiconductor) when used as a working electrode in a PEC cell, different from a TaON electrode that essentially gave only an n-type response (Figure 15D).¹⁰⁴ In an n-type semiconductor photocatalyst, electrons tend to accumulate in the bulk, while holes undergo localization on the surface, due to the band bending characteristics with respect to aqueous solution.⁴ Recombination between bulk electrons and surface holes would therefore be the dominant path in an n-type semiconductor photocatalyst suspended in an aqueous solution.⁸⁸ In addition, intrinsic electrons existing in the bulk of an n-type semiconductor have a significant impact on charge recombination. Accordingly, moderation of the n-type semiconducting character of TaON is expected to suppress recombination, resulting in high photocatalytic performance. This idea is consistent with our recent study of a kinetic model of a photocatalytic water-splitting mechanism on GaN:ZnO powder, which is an n-type semiconductor. Thus, moderation of the n-type semiconducting character of TaON by the formation of a composite with ZrO₂ is another possible reason for the high photocatalytic activity of ZrO₂/TaON.

4.3.4 Application to Z-scheme Water Splitting: Because the enhanced performance of ZrO₂/TaON for water reduction is attractive for use as a H₂ evolution photocatalyst in a Z-scheme water-splitting system, a Z-scheme water-splitting system consisting of ZrO₂/TaON (H₂ evolution photocatalyst), an O₂ evolution photocatalyst, and a redox mediator was investigated. Among the O₂ evolution photocatalysts and redox mediators examined, PtO_x/WO₃ and an IO₃⁻/I⁻ couple were

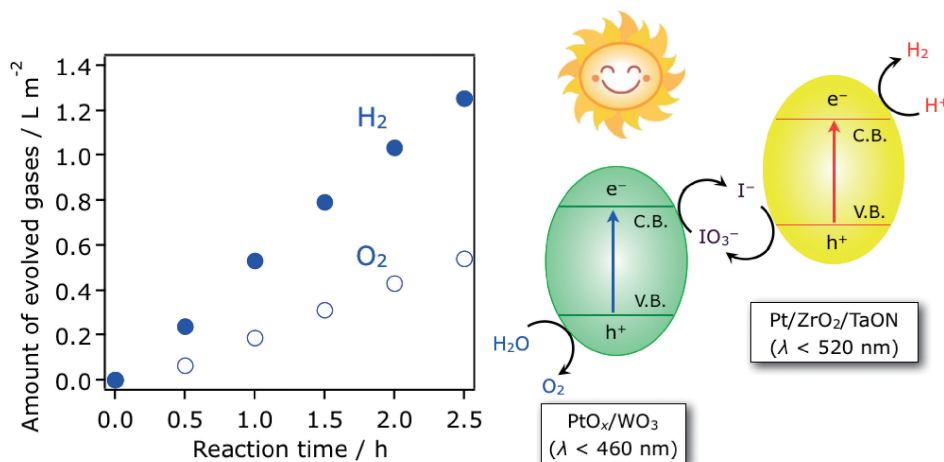


Figure 17. Z-scheme water splitting over a mixture of PtO_x/WO₃ (50 mg) and Pt/ZrO₂/TaON (25 mg) from an aqueous NaI solution (0.5 mM, 100 mL) under simulated sunlight (100 mW cm⁻²). Irradiation area: 16 cm².

the most effective components, respectively. Stoichiometric water splitting into H₂ and O₂ was accomplished by combining these two components with Pt-loaded ZrO₂/TaON, recording an AQY of 6.3% with 420 nm monochromatic light. This value was at least 6 times greater than the yield achieved using a TaON analogue, and one of the highest ones among reported visible-light-driven water-splitting systems.

Overall water splitting under simulated sunlight (100 mW cm⁻²) was also achieved using the optimized Pt/ZrO₂/TaON photocatalyst in the same Z-scheme system, as shown in Figure 17. Here solar-to-hydrogen energy conversion efficiency was calculated to be 0.19 ± 0.02%, almost the same as the efficiency of natural photosynthesis in switchgrass (0.2%),¹⁰⁵ which is considered to be a promising plant for biomass energy production. Thus, it was experimentally shown that an artificial photosynthetic assembly could be realized with the use of carefully designed inorganic compounds.

The performance of a similar Z-scheme system consisting of Pt/TaON (for H₂ evolution) and RuO₂/TaON (for O₂ evolution) in the presence of an IO₃⁻/I⁻ shuttle redox mediator was also improved by simply replacing Pt/TaON with Pt/ZrO₂/TaON, giving 6–7-fold activity enhancement.^{10,91} In addition, when ZrO₂/TaON was employed in the H₂ evolution system, one could extend the wavelength available for O₂ evolution by applying Ta₃N₅ that has an absorption edge of ca. 600 nm.¹⁰⁶

4.3.5 Overall Water Splitting Using ZrO₂/TaON Modified with Water Reduction/Oxidation Cocatalysts: To achieve overall water splitting without any redox mediator, the optimized ZrO₂/TaON was further modified with suitable water reduction/oxidation cocatalysts. Hara et al. investigated the effect of cocatalyst-loading on photocatalytic H₂ evolution by TaON.¹⁸ According to that study, photodeposition of Ru on TaON resulted in marked enhancement in activity, despite the fact that the overpotential of Ru for H₂ evolution is not very small, suggesting the importance of interfacial electron transfer between TaON and Ru.

We therefore photodeposited Ru as the component of the H₂ evolution site on ZrO₂/TaON. XPS analysis showed that the deposited Ru species were slightly oxidized relative to Ru metal, but not as much as a bulk RuO₂ reference. Here, we will

represent the Ru species as RuO_x for simplicity. TEM images of RuO_x/ZrO₂/TaON indicated that the primary particle size of introduced RuO_x nanoparticles was 1–2 nm, but some of them aggregated to form larger secondary particles (ca. 5 nm).

In order to suppress possible backward reactions such as H₂–O₂ recombination and O₂ photoreduction that can occur on RuO_x, a Cr₂O₃ shell was coated on RuO_x according to our previous methodology. The as-prepared RuO_x-core/Cr₂O₃-shell nanoparticles were employed as the H₂ evolution site on ZrO₂/TaON. TEM observation revealed that the RuO_x nanoparticles were coated with a shell layer of ca. 1–2 nm in thickness, forming a core/shell nanostructure. However, some of the RuO_x nanoparticles on both the TaON- and ZrO₂-components remained uncovered.¹⁰⁷ This is presumably because part of the RuO_x nanoparticles work as active sites for oxidation reactions, as discussed earlier.

As displayed in Figure 18A, RuO_x-loaded ZrO₂/TaON showed little photocatalytic activity, producing only H₂ at a moderate rate. On the other hand, modification of RuO_x/ZrO₂/TaON with Cr₂O₃ resulted in simultaneous H₂ and O₂ evolution from pure water. However, the rates of H₂ and O₂ evolution decreased with time, likely due to the oxidative decomposition of the nitride component by photogenerated holes as follows:



The deactivation could be suppressed upon decoration with 1–2 nm colloidal IrO₂, which is well known as an efficient water oxidation cocatalyst. A similarly prepared material without Cr₂O₃ exhibited moderate H₂ evolution, but no O₂ under the same reaction conditions, which indicated the vital role of the Cr₂O₃ shell in realizing overall water splitting. Neither H₂ nor O₂ was produced from ZrO₂/TaON modified only with IrO₂ colloids as well.

Visible-light-driven overall water splitting was finally achieved using ZrO₂/TaON modified with core/shell-structured nanoparticles of RuO_x/Cr₂O₃ and colloidal IrO₂ as H₂ and O₂ evolution sites, as shown in Figure 18B. This was the first example of a d⁰-type non-oxide photocatalyst that achieves direct splitting of pure water into H₂ and O₂ only with visible light. Obviously, it was important to improve the quality of the

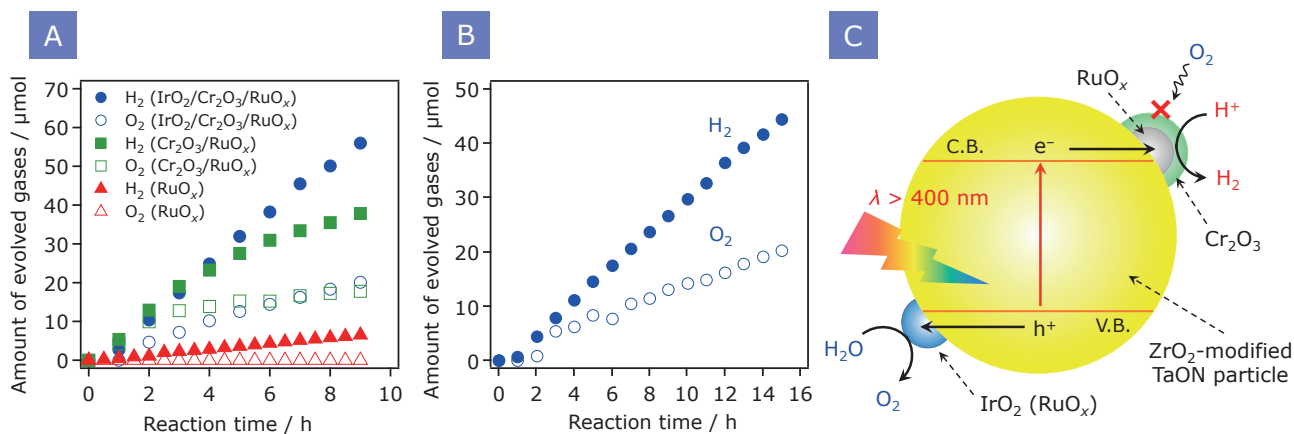


Figure 18. (A) Overall water splitting using ZrO₂/TaON with various modifications under UV irradiation (>300 nm). (B) Typical time course of overall water splitting visible light (λ > 400 nm) on IrO₂/Cr₂O₃/RuO_x/ZrO₂/TaON, and (C) the proposed reaction mechanism. Reproduced from ref 107 with permission.

photocatalyst (i.e., TaON modified with ZrO₂ to reduce the density of defects) and to construct suitable surface reaction sites on the photocatalyst. In this case, H₂ evolution sites that are insensitive to O₂ photoreduction, and O₂ evolution sites that efficiently promote water oxidation while suppressing the oxidative decomposition of the material, were both essential (Figure 18C).

4.4 BaZrO₃–BaTaO₂N Solid Solution Operable under a Wide Range of Visible Light. Because ZrO₂/TaON harvests visible light only up to 520 nm, utilization of a wide range of visible light is highly desirable. By applying a similar strategy to ZrO₂/TaON, BaTaO₂N having an absorption edge at 660 nm was modified by BaZrO₃ that has the same perovskite structure as BaTaO₂N in order to reduce the density of anionic defects. Although the obtained material was not a composite of BaZrO₃ and BaTaO₂N but a solid solution between the two, an enhanced activity for H₂ evolution in a non-sacrificial system (7–8-fold enhancement) was obtained.¹⁰⁸ Using the optimized BaZrO₃–BaTaO₂N solid solution combined with a suitable O₂ evolution photocatalyst (e.g., rutile TiO₂ and PtO_x/WO₃), solar-driven Z-scheme water splitting was also accomplished in the presence of an IO₃⁻/I⁻ redox couple.¹⁰⁹

In contrast to the H₂ evolution activity of BaTaO₂N, it had been reported that BaTaO₂N is unable to catalyze water oxidation under visible light even in the presence of an electron acceptor like Ag⁺.²⁹ As the band gap of a given material is decreased, the driving forces for water oxidation and reduction should inevitably decrease, making water splitting more difficult. Hence, one might regard BaTaO₂N unsuitable for applications in light-driven water splitting. Contrary to the previous report, we demonstrated that carefully prepared BaZrO₃–BaTaO₂N solid solutions having single-phase perovskite structures are active for both water reduction and oxidation even under >660 nm irradiation.¹¹⁰ This was the first demonstration that a semiconductor having an absorption edge longer than 600 nm achieves functionality as a photocatalyst to reduce and oxidize water under visible light. Importantly, BaZrO₃–BaTaO₂N solid solution also worked as a photocatalyst to oxidize water into O₂ and reduce IO₃⁻ into I⁻, meaning that it is possible to create a Z-scheme water-splitting

system consisting only of BaZrO₃–BaTaO₂N having a 660 nm absorption edge.¹⁰⁹ It was also found that BaZrO₃–BaTaO₂N solid solution showed an enhanced activity for not only water reduction but also water oxidation compared to BaTaO₂N,^{110,111} and could be applicable to a photoanode material for solar water oxidation that works even in a two-electrode configuration and in the presence of an applied bias (+1.0 V vs. Pt wire cathode).¹¹⁰

Similar to overall water splitting using ZrO₂/TaON, modification of BaZrO₃–BaTaO₂N with IrO₂ colloidal nanoparticles was indispensable to achieving stable water oxidation. Without IrO₂, BaZrO₃–BaTaO₂N released N₂ upon band-gap irradiation due to self-oxidative decomposition while producing a small amount of O₂. Nevertheless, the AQY of the optimized IrO₂/BaZrO₃–BaTaO₂N for water oxidation was below 0.1% at 420 nm, at least an order of magnitude lower than those recorded using similar (oxy)nitrides having a 600 nm absorption edge (e.g., LaTiO₂N, Ta₃N₅). In order to elucidate the reason for the low water oxidation activity of BaZrO₃–BaTaO₂N, we estimated the band-edge potentials by means of a PEC technique and UV–visible diffuse reflectance spectroscopy.¹¹¹ Figure 19 shows the estimated conduction and valence band edge potentials of BaZrO₃–BaTaO₂N (Ba/Zr = 0.025) as a function of pH. The positions of the CBM and the VBM of BaZrO₃–BaTaO₂N are dependent on pH, with a variation of approximately –50 mV per pH decade. The estimated band edge positions of the BaZrO₃–BaTaO₂N solid solution straddle water reduction and oxidation potentials, in agreement with the results of photocatalytic reactions, as mentioned above. However, it should be noted that the energy difference between the water oxidation potential and the VBM is at most 0.3 eV, smaller than those of other (oxy)nitride materials.¹¹¹ This would lead to a relatively low AQY of the material for water oxidation.

4.5 Unusual Enhancement of Water Oxidation Activity of BaTaO₂N by Doping of Pentavalent Tungsten Species. It was thus experimentally demonstrated that the reduction and oxidation of water are both possible using perovskite BaTaO₂N and solid-solution materials with BaZrO₃ (0 < Zr/Ta ≤ 0.1) that have band gaps of 1.7–1.8 eV.¹¹⁰ However, the BaZrO₃–

BaTaO₂N solid solutions have a drawback in that the water oxidation activity is very low, likely due to the valence band potential that is located at a potential close to the water oxidation potential. Here, one may think that it is possible to tune the band-edge positions of a semiconductor by replacing the original constituent element with another.³ For BaTaO₂N, it would be easy to expect that the VBM shifts to more positive potential if the concentration of nitrogen, which forms the upper part of the valence band,² is reduced. This is actually achievable by making a solid solution with a wide-gap oxide, which is generally known as “band-gap engineering”,³ as we have shown with BaZrO₃–BaTaO₂N solid solutions. From the viewpoint of efficient solar energy utilization, however, this may not be preferable because the reduction of the nitrogen concentration in BaTaO₂N results in a blue shift of the absorption edge, downgrading the good light absorption capability.¹¹⁰

We accidentally found that the water oxidation activity of BaTaO₂N photocatalyst can be enhanced by the introduction of pentavalent tungsten species, while maintaining the small band gap.¹¹² Figure 20A shows UV–visible diffuse reflectance spectra of W-doped BaTaO₂N samples prepared in a similar manner to BaZrO₃–BaTaO₂N. Besides the original absorption

edge at 660 nm, the doped samples had an additional absorption band at a longer wavelength region, which was more pronounced with an increase in the W/Ta molar ratio in the sample. This absorption band can be assigned to pentavalent W species. In general, doping transition-metal cations having partly filled d orbitals into semiconductor photocatalysts contributes to a significant drop in photocatalytic activity.³ Such doped elements form a donor or acceptor level in the forbidden band of the material, which may act as a center for absorption at visible wavelengths on a case-by-case basis. However, doping also obstructs prompt migration of photo-generated electrons or holes at the surface and in the bulk material, since the dopant frequently provides a discreet energy level rather than an energy band. Nevertheless, as shown in Figure 20B, the water oxidation activity of BaTaO₂N was improved by introducing a small amount of W species to reach a maximum at a W/Ta molar ratio of 0.005, beyond which it began to drop. The optimized W-doped BaTaO₂N exhibited an activity 7 times higher than BaTaO₂N under the same reaction conditions (Figure 20C). It was also higher than the optimized BaZrO₃–BaTaO₂N. Although the reason for the enhanced activity has not been fully understood, the finding that an intentional introduction of transition-metal cations with partly filled d orbitals into a narrow-gap oxynitride improves the water oxidation activity presents important new possibilities for the photocatalysis of visible-light water oxidation, as there are many (oxy)nitrides that can absorb visible photons to oxidize water.

5. Summary

Metal (oxy)nitrides have attracted attention as photocatalysts for overall water splitting under visible irradiation. We developed solid solutions of GaN and ZnO with d¹⁰ electronic configuration, which achieved functionality as stable photocatalysts to split water into H₂ and O₂ by absorbing up to 500 nm photons. This is the first successful example of “reproducible” overall water splitting using a single semiconductor photocatalyst and visible light.

During the development of the GaN:ZnO photocatalyst, we also devised a new type of cocatalyst: Cr(III)-containing mixed oxides and core/shell-structured metal (or metal-oxide)/Cr₂O₃

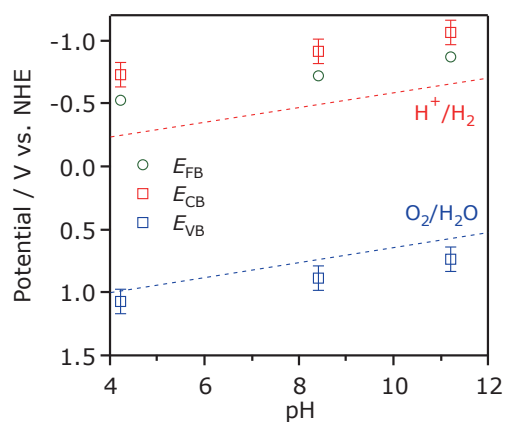


Figure 19. Dependence of conduction and valence band edge potentials for BaZrO₃–BaTaO₂N (Zr/Ta = 0.025) on pH of electrolyte, as determined from photocurrent measurements. Reproduced from ref 111 with permission.

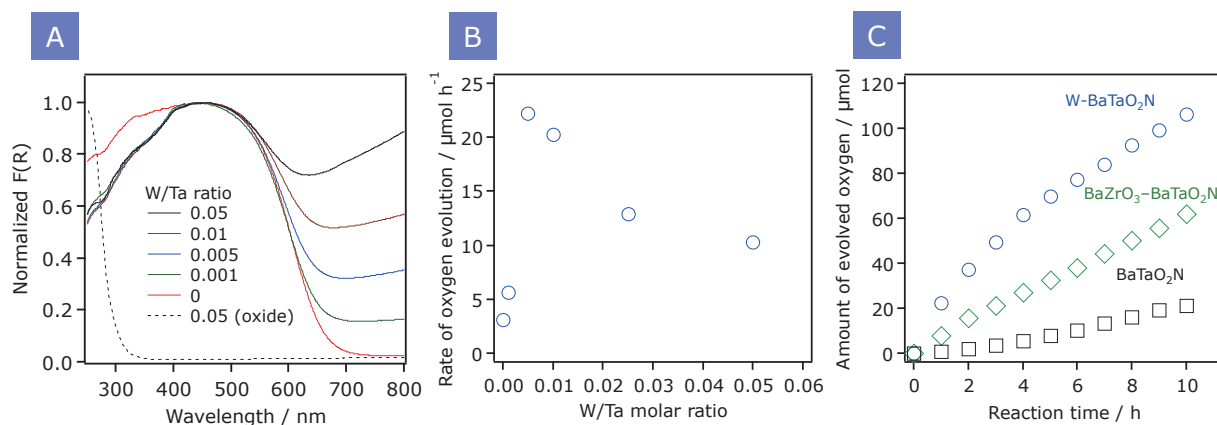


Figure 20. (A) Diffuse reflectance spectra and (B) photocatalytic water oxidation activities of W-doped BaTaO₂N. (C) Comparison of photocatalytic performance. The reactions were conducted in an aqueous AgNO₃ solution under visible light ($\lambda > 420$ nm) using 100 mg of each sample (1.5 wt % IrO₂ loaded) and 200 mg of La₂O₃. Reproduced from ref 112 with permission.

nanoparticles, which promote H₂ evolution while suppressing undesirable backward reactions (e.g., water formation and O₂ photoreduction), resulting in a drastic enhancement in photocatalytic activity of GaN:ZnO for overall water splitting. It was also demonstrated that modification of a photocatalyst with two different cocatalysts for H₂ and O₂ evolution resulted in enhanced performance compared to photocatalysts modified with either an H₂ or O₂ evolution cocatalyst.

While (oxy)nitrides having d⁰-electronic configuration are capable of absorbing a wide range of visible light, reducing the density of anionic defects that are generated during the synthesis was found to be indispensable to inducing the potential of these materials for overall water splitting. In particular, TaON modified with nanoparticulate ZrO₂ exhibited an enhanced activity for H₂ evolution, leading to efficient Z-scheme water splitting with ca. 0.2% solar energy conversion efficiency. Stoichiometric water splitting under visible light was accomplished using the optimized ZrO₂/TaON photocatalyst modified with two different cocatalysts for H₂ and O₂ evolution, which represents the first demonstration of overall water splitting using a d⁰-type oxynitride.

All of the successful photocatalysts developed for overall water splitting before 2005 comprised solely metal oxides that are largely insensitive to visible light. The discovery of oxynitrides achieving the same function motivated us to expand our research toward both practical application and fundamental understanding of such materials. Unfortunately, however, the conversion efficiencies in photocatalytic water splitting are still low, most likely due to electron-hole recombination that still occurs significantly both in the bulk and surface of photocatalysts. Further research is thus required to improve the conversion efficiencies of (oxy)nitrides.

The authors acknowledge their co-workers whose names appear in the cited references. The research described herein was supported by a Grant-in-Aid for JSPS fellows, a PRESTO/JST program (Chemical Conversion of Light Energy), the 21st Century Center of Excellence (COE), and the Research and Development in a New Interdisciplinary Field Based on Nanotechnology and Materials Science programs of the Ministry of Education, Culture, Sports, Science and Technology (MEXT) of Japan. Acknowledgment is also extended to the KAITEKI Institute, Inc., the Global Center of Excellence (GCOE) Program for Chemistry Innovation through Cooperation of Science and Engineering and Nippon Sheet Glass Foundation for Materials Science and Engineering.

References

- J. S. Lee, *Catal. Surv. Asia* **2005**, *9*, 217.
- K. Maeda, K. Domen, *J. Phys. Chem. C* **2007**, *111*, 7851.
- A. Kudo, Y. Miseki, *Chem. Soc. Rev.* **2009**, *38*, 253.
- R. Abe, *J. Photochem. Photobiol., C* **2010**, *11*, 179.
- R. Abe, *Bull. Chem. Soc. Jpn.* **2011**, *84*, 1000.
- K. Maeda, *J. Photochem. Photobiol., C* **2011**, *12*, 237.
- Y. Wang, X. Wang, M. Antonietti, *Angew. Chem., Int. Ed.* **2012**, *51*, 68.
- F. E. Osterloh, *Chem. Soc. Rev.* **2013**, *42*, 2294.
- K. Maeda, *ACS Catal.* **2013**, *3*, 1486.
- K. Maeda, *Phys. Chem. Chem. Phys.* **2013**, *15*, 10537.
- A. Fujishima, K. Honda, *Nature* **1972**, *238*, 37.
- M. Grätzel, *Nature* **2001**, *414*, 338.
- K. Sivula, F. Le Formal, M. Grätzel, *ChemSusChem* **2011**, *4*, 432.
- S. Sato, J. M. White, *Chem. Phys. Lett.* **1980**, *72*, 83.
- K. Domen, S. Naito, M. Soma, T. Onishi, K. Tamaru, *J. Chem. Soc., Chem. Commun.* **1980**, 543.
- J. M. Lehn, J. P. Sauvage, R. Ziessel, *Nouv. J. Chim.* **1980**, *4*, 623.
- K. Maeda, K. Domen, *J. Phys. Chem. Lett.* **2010**, *1*, 2655.
- M. Hara, J. Nunoshige, T. Takata, J. N. Kondo, K. Domen, *Chem. Commun.* **2003**, 3000.
- H. G. Kim, D. W. Hwang, J. Kim, Y. G. Kim, J. S. Lee, *Chem. Commun.* **1999**, 1077.
- H. Kato, A. Kudo, *J. Phys. Chem. B* **2001**, *105*, 4285.
- H. Kato, K. Asakura, A. Kudo, *J. Am. Chem. Soc.* **2003**, *125*, 3082.
- Y. Miseki, H. Kato, A. Kudo, *Energy Environ. Sci.* **2009**, *2*, 306.
- Y. Sakata, T. Hayashi, R. Yasunaga, N. Yanaga, H. Imamura, *Chem. Commun.* **2015**, *51*, 12935.
- D. E. Scaife, *Sol. Energy* **1980**, *25*, 41.
- R. Asahi, T. Morikawa, T. Ohwaki, K. Aoki, Y. Taga, *Science* **2001**, *293*, 269.
- M. Jansen, H. P. Letschert, *Nature* **2000**, *404*, 980.
- G. Hitoki, T. Takata, J. N. Kondo, M. Hara, H. Kobayashi, K. Domen, *Chem. Commun.* **2002**, 1698.
- G. Hitoki, A. Ishikawa, T. Takata, J. N. Kondo, M. Hara, K. Domen, *Chem. Lett.* **2002**, 736.
- G. Hitoki, T. Takata, J. N. Kondo, M. Hara, H. Kobayashi, K. Domen, *Electrochemistry* **2002**, *70*, 463.
- A. Kasahara, K. Nukumizu, G. Hitoki, T. Takata, J. N. Kondo, M. Hara, H. Kobayashi, K. Domen, *J. Phys. Chem. A* **2002**, *106*, 6750.
- Here a photocatalyst that contains such transition-metal cations (e.g., Ti⁴⁺, Nb⁵⁺, or Ta⁵⁺) is defined as a “d⁰ electronic configuration” photocatalyst, while photocatalysts that contain typical metal cations (e.g., Ga³⁺ and Ge⁴⁺) with a filled d orbital are defined as “d¹⁰ electronic configuration” photocatalysts.
- A. J. Bard, M. A. Fox, *Acc. Chem. Res.* **1995**, *28*, 141.
- Y. Inoue, *Energy Environ. Sci.* **2009**, *2*, 364.
- J. Sato, N. Saito, Y. Yamada, K. Maeda, T. Takata, J. N. Kondo, M. Hara, H. Kobayashi, K. Domen, Y. Inoue, *J. Am. Chem. Soc.* **2005**, *127*, 4150.
- Y. Lee, T. Watanabe, T. Takata, M. Hara, M. Yoshimura, K. Domen, *J. Phys. Chem. B* **2006**, *110*, 17563.
- K. Maeda, N. Saito, D. Lu, Y. Inoue, K. Domen, *J. Phys. Chem. C* **2007**, *111*, 4749.
- K. Maeda, N. Saito, Y. Inoue, K. Domen, *Chem. Mater.* **2007**, *19*, 4092.
- S. S. Kocha, M. W. Peterson, D. J. Arent, J. M. Redwing, M. Tischler, J. A. Turner, *J. Electrochem. Soc.* **1995**, *142*, L238.
- I. M. Huygens, K. Strubbe, W. P. Gomes, *J. Electrochem. Soc.* **2000**, *147*, 1797.
- J. D. Beach, R. T. Collins, J. A. Turner, *J. Electrochem. Soc.* **2003**, *150*, A899.
- S.-H. Wei, A. Zunger, *Phys. Rev. B* **1988**, *37*, 8958.
- H. Schulz, K. H. Thiemann, *Solid State Commun.* **1977**, *23*, 815.
- O. Garcia-Martinez, R. M. Rojas, E. Vila, J. L. Martin de Vidales, *Solid State Ionics* **1997**, *63*, 442.
- K. Maeda, T. Takata, M. Hara, N. Saito, Y. Inoue, H.

- Kobayashi, K. Domen, *J. Am. Chem. Soc.* **2005**, *127*, 8286.
- 45 K. Maeda, K. Teramura, T. Takata, M. Hara, N. Saito, K. Toda, Y. Inoue, H. Kobayashi, K. Domen, *J. Phys. Chem. B* **2005**, *109*, 20504.
- 46 M. Yashima, K. Maeda, K. Teramura, T. Takata, K. Domen, *Chem. Phys. Lett.* **2005**, *416*, 225.
- 47 T. Hirai, K. Maeda, M. Yoshida, J. Kubota, S. Ikeda, M. Matsumura, K. Domen, *J. Phys. Chem. C* **2007**, *111*, 18853.
- 48 M. Yoshida, T. Hirai, K. Maeda, N. Saito, J. Kubota, H. Kobayashi, Y. Inoue, K. Domen, *J. Phys. Chem. C* **2010**, *114*, 15510.
- 49 K. Maeda, K. Domen, *Chem. Mater.* **2010**, *22*, 612.
- 50 H. Gerischer, *J. Electrochem. Soc.* **1966**, *113*, 1174.
- 51 X. Sun, K. Maeda, M. Le Faucheur, K. Teramura, K. Domen, *Appl. Catal., A* **2007**, *327*, 114.
- 52 T. Hisatomi, K. Maeda, D. Lu, K. Domen, *ChemSusChem* **2009**, *2*, 336.
- 53 K. Maeda, H. Hashiguchi, H. Masuda, R. Abe, K. Domen, *J. Phys. Chem. C* **2008**, *112*, 3447.
- 54 C. T. K. Thaminimulla, T. Takata, M. Hara, J. N. Kondo, K. Domen, *J. Catal.* **2000**, *196*, 362.
- 55 K. Maeda, K. Teramura, D. Lu, T. Takata, N. Saito, Y. Inoue, K. Domen, *Nature* **2006**, *440*, 295.
- 56 K. Maeda, K. Teramura, H. Masuda, T. Takata, N. Saito, Y. Inoue, K. Domen, *J. Phys. Chem. B* **2006**, *110*, 13107.
- 57 K. Maeda, K. Teramura, D. Lu, T. Takata, N. Saito, Y. Inoue, K. Domen, *J. Phys. Chem. B* **2006**, *110*, 13753.
- 58 K. Maeda, K. Teramura, N. Saito, Y. Inoue, K. Domen, *J. Catal.* **2006**, *243*, 303.
- 59 K. Maeda, T. Ohno, K. Domen, *Chem. Sci.* **2011**, *2*, 1362.
- 60 K. Domen, A. Kudo, T. Onishi, *J. Catal.* **1986**, *102*, 92.
- 61 K. Sayama, H. Arakawa, *J. Chem. Soc., Faraday Trans.* **1997**, *93*, 1647.
- 62 K. Sayama, H. Arakawa, *J. Photochem. Photobiol., A* **1996**, *94*, 67.
- 63 K. Maeda, H. Masuda, K. Domen, *Catal. Today* **2009**, *147*, 173.
- 64 R. Abe, K. Sayama, H. Sugihara, *J. Phys. Chem. B* **2005**, *109*, 16052.
- 65 R. Abe, T. Takata, H. Sugihara, K. Domen, *Chem. Commun.* **2005**, 3829.
- 66 T. Ohno, L. Bai, T. Hisatomi, K. Maeda, K. Domen, *J. Am. Chem. Soc.* **2012**, *134*, 8254.
- 67 K. Maeda, K. Teramura, N. Saito, Y. Inoue, K. Domen, *Bull. Chem. Soc. Jpn.* **2007**, *80*, 1004.
- 68 Y. Lee, K. Teramura, M. Hara, K. Domen, *Chem. Mater.* **2007**, *19*, 2120.
- 69 K. Maeda, D. Lu, K. Teramura, K. Domen, *J. Mater. Chem.* **2008**, *18*, 3539.
- 70 K. Maeda, D. Lu, K. Teramura, K. Domen, *Energy Environ. Sci.* **2010**, *3*, 471.
- 71 H. J. Lugo, J. H. Lunsford, *J. Catal.* **1985**, *91*, 155.
- 72 G. Busca, *J. Catal.* **1989**, *120*, 303.
- 73 B. Sun, E. P. Reddy, P. G. Smirniotis, *Environ. Sci. Technol.* **2005**, *39*, 6251.
- 74 K. Maeda, K. Teramura, D. Lu, N. Saito, Y. Inoue, K. Domen, *Angew. Chem., Int. Ed.* **2006**, *45*, 7806.
- 75 K. Maeda, K. Teramura, D. Lu, N. Saito, Y. Inoue, K. Domen, *J. Phys. Chem. C* **2007**, *111*, 7554.
- 76 K. Maeda, N. Sakamoto, T. Ikeda, H. Ohtsuka, A. Xiong, D. Lu, M. Kanehara, T. Teranishi, K. Domen, *Chem.—Eur. J.* **2010**, *16*, 7750.
- 77 M. Yoshida, K. Takanabe, K. Maeda, A. Ishikawa, J. Kubota, Y. Sakata, Y. Ikezawa, K. Domen, *J. Phys. Chem. C* **2009**, *113*, 10151.
- 78 J. J. Testa, M. A. Grela, M. I. Litter, *Langmuir* **2001**, *17*, 3515.
- 79 T. P. Moffat, H. Yang, F.-R. F. Fan, A. J. Bard, *J. Electrochem. Soc.* **1992**, *139*, 3158.
- 80 N. Sakamoto, H. Ohtsuka, T. Ikeda, K. Maeda, D. Lu, M. Kanehara, K. Teramura, T. Teranishi, K. Domen, *Nanoscale* **2009**, *1*, 106.
- 81 T. Ikeda, A. Xiong, T. Yoshinaga, K. Maeda, K. Domen, T. Teranishi, *J. Phys. Chem. C* **2013**, *117*, 2467.
- 82 Y. Negishi, M. Mizuno, M. Hirayama, M. Omatoi, T. Takayama, A. Iwase, A. Kudo, *Nanoscale* **2013**, *5*, 7188.
- 83 K. Maeda, A. Xiong, T. Yoshinaga, T. Ikeda, N. Sakamoto, T. Hisatomi, M. Takashima, D. Lu, M. Kanehara, T. Setoyama, T. Teranishi, K. Domen, *Angew. Chem., Int. Ed.* **2010**, *49*, 4096.
- 84 A. Harriman, I. J. Pickering, J. M. Thomas, P. A. Christensen, *J. Chem. Soc., Faraday Trans. 1* **1988**, *84*, 2795.
- 85 Y. Umena, K. Kawakami, J.-R. Shen, N. Kamiya, *Nature* **2011**, *473*, 55.
- 86 B. Kraetler, A. J. Bard, *J. Am. Chem. Soc.* **1978**, *100*, 4317.
- 87 A. Xiong, T. Yoshinaga, T. Ikeda, M. Takashima, T. Hisatomi, K. Maeda, T. Setoyama, T. Teranishi, K. Domen, *Eur. J. Inorg. Chem.* **2014**, 767.
- 88 T. Hisatomi, K. Maeda, K. Takanabe, J. Kubota, K. Domen, *J. Phys. Chem. C* **2009**, *113*, 21458.
- 89 S. S. K. Ma, K. Maeda, R. Abe, K. Domen, *Energy Environ. Sci.* **2012**, *5*, 8390.
- 90 A. J. Bard, *J. Photochem.* **1979**, *10*, 59.
- 91 K. Maeda, R. Abe, K. Domen, *J. Phys. Chem. C* **2011**, *115*, 3057.
- 92 M. Higashi, R. Abe, K. Teramura, T. Takata, B. Ohtani, K. Domen, *Chem. Phys. Lett.* **2008**, *452*, 120.
- 93 M. Higashi, R. Abe, A. Ishikawa, T. Takata, B. Ohtani, K. Domen, *Chem. Lett.* **2008**, *37*, 138.
- 94 K. Maeda, N. Nishimura, K. Domen, *Appl. Catal., A* **2009**, *370*, 88.
- 95 L. Yuliati, J.-H. Yang, X. Wang, K. Maeda, T. Takata, M. Antonietti, K. Domen, *J. Mater. Chem.* **2010**, *20*, 4295.
- 96 R. Sasaki, K. Maeda, Y. Kako, K. Domen, *Appl. Catal., B* **2012**, *128*, 72.
- 97 K. Maeda, H. Terashima, K. Kase, K. Domen, *Appl. Catal., A* **2009**, *357*, 206.
- 98 K. Sayama, H. Arakawa, K. Domen, *Catal. Today* **1996**, *28*, 175.
- 99 H. Kominami, S. Murakami, Y. Kera, B. Ohtani, *Catal. Lett.* **1998**, *56*, 125.
- 100 K. Maeda, K. Teramura, K. Domen, *J. Catal.* **2008**, *254*, 198.
- 101 R. Abe, T. Takata, H. Sugihara, K. Domen, *Chem. Lett.* **2005**, *34*, 1162.
- 102 K. Maeda, H. Terashima, K. Kase, M. Higashi, M. Tabata, K. Domen, *Bull. Chem. Soc. Jpn.* **2008**, *81*, 927.
- 103 S. S. K. Ma, K. Maeda, K. Domen, *Catal. Sci. Technol.* **2012**, *2*, 818.
- 104 K. Maeda, M. Higashi, D. Lu, R. Abe, K. Domen, *J. Am. Chem. Soc.* **2010**, *132*, 5858.
- 105 I. Lewandowski, J. M. O. Scurlock, E. Lindvall, M. Christou, *Biomass Bioenergy* **2003**, *25*, 335.
- 106 M. Tabata, K. Maeda, M. Higashi, D. Lu, T. Takata, R.

- Abe, K. Domen, *Langmuir* **2010**, *26*, 9161.
- 107 K. Maeda, D. Lu, K. Domen, *Chem.—Eur. J.* **2013**, *19*, 4986.
- 108 T. Matoba, K. Maeda, K. Domen, *Chem.—Eur. J.* **2011**, *17*, 14731.
- 109 K. Maeda, D. Lu, K. Domen, *ACS Catal.* **2013**, *3*, 1026.
- 110 K. Maeda, K. Domen, *Angew. Chem., Int. Ed.* **2012**, *51*, 9865.
- 111 K. Maeda, K. Domen, *J. Catal.* **2014**, *310*, 67.
- 112 K. Maeda, D. Lu, K. Domen, *Angew. Chem., Int. Ed.* **2013**, *52*, 6488.